

PATH-CONSERVATIVE CENTRAL-UPWIND SCHEMES FOR NONCONSERVATIVE HYPERBOLIC SYSTEMS

MANUEL JESÚS CASTRO DÍAZ¹ AND ALEXANDER KURGANOV^{2,3,*},
AND TOMÁS MORALES DE LUNA⁴

Abstract. We develop path-conservative central-upwind schemes for nonconservative one-dimensional hyperbolic systems of nonlinear partial differential equations. Such systems arise in a variety of applications and the most challenging part of their numerical discretization is a robust treatment of nonconservative product terms. Godunov-type central-upwind schemes were developed as an efficient, highly accurate and robust “black-box” solver for hyperbolic systems of conservation and balance laws. They were successfully applied to a large number of hyperbolic systems including several nonconservative ones. To overcome the difficulties related to the presence of nonconservative product terms, several special techniques were proposed. However, none of these techniques was sufficiently robust and thus the applicability of the original central-upwind schemes was rather limited. In this paper, we rewrite the central-upwind schemes in the form of path-conservative schemes. This helps us (i) to show that the main drawback of the original central-upwind approach was the fact that the jump of the nonconservative product terms across cell interfaces has never been taken into account and (ii) to understand how the nonconservative products should be discretized so that their influence on the numerical solution is accurately taken into account. The resulting path-conservative central-upwind scheme is a new robust tool for both conservative and nonconservative hyperbolic systems. We apply the new scheme to the Saint-Venant system with discontinuous bottom topography and two-layer shallow water system. Our numerical results illustrate the good performance of the new path-conservative central-upwind scheme, its robustness and ability to achieve very high resolution.

Mathematics Subject Classification. 76M12, 65M08, 35L65, 35L67, 86-08.

Received April 10, 2018. Accepted December 20, 2018.

1. INTRODUCTION

This paper is focused on development of path-conservative central-upwind (PCCU) schemes for nonconservative one-dimensional (1D) hyperbolic system of nonlinear partial differential equations (PDEs),

Keywords and phrases. Nonconservative hyperbolic systems of PDEs, Saint-Venant system, two-layer shallow water equations, central-upwind scheme, path-conservative scheme, well-balanced scheme.

¹ Departamento de Análisis Matemático, Universidad de Málaga, 29080 Málaga, Spain.

² Department of Mathematics, Southern University of Science and Technology, 518055 Shenzhen, China.

³ Mathematics Department, Tulane University, New Orleans, LA 70118, USA.

⁴ Departamento de Matemáticas, Universidad de Córdoba, Campus de Rabanales, 14071 Córdoba, Spain.

*Corresponding author: kurganov@math.tulane.edu

$$\mathbf{U}_t + \mathbf{F}(\mathbf{U})_x = B(\mathbf{U})\mathbf{U}_x, \quad B \in \mathbb{R}^{N \times N}, \quad (1.1)$$

where $\mathbf{U} \in \mathbb{R}^N$ is a vector of unknown quantities, $\mathbf{F} : \mathbb{R}^N \rightarrow \mathbb{R}^N$ is a (nonlinear) flux, and $B(\mathbf{U}) \in \mathbb{R}^{N \times N}$.

PDE systems of this form arise in many fluid models in different contexts: Saint-Venant system of shallow water equations with arbitrary bottom topography, multilayer shallow water models, multiphase flow models and many others.

Central-upwind (CU) schemes were originally introduced in [34, 38] (see also [30, 32]) for 1D hyperbolic systems of conservation laws,

$$\mathbf{U}_t + \mathbf{F}(\mathbf{U})_x = \mathbf{0}, \quad (1.2)$$

and its multidimensional extensions. CU schemes belong to the class of Riemann-problem-solver-free Godunov-type central schemes; see [24, 40, 52], where the simplest first- and second-order central schemes were introduced, and [30] for a recent review of central schemes. Therefore, CU schemes enjoy the main advantages of central schemes – *simplicity* and *robustness*. As CU schemes do not use any (approximate) Riemann problem solvers or local characteristic decomposition, they can be used as “black-box” solvers for general multidimensional hyperbolic systems of conservation laws. At the same time, CU scheme have a certain upwind nature as the information on local speeds of propagation (related to the largest and smallest eigenvalues of the Jacobian $\partial\mathbf{F}/\partial\mathbf{U}$) are used in their derivation to reduce excessive numerical dissipation (see, e.g., [30, 32, 34, 37, 38]) typically present in staggered central schemes such as the Nessyahu-Tadmor scheme [52] and its higher-order (see, e.g., [6, 44, 47]) and multidimensional (see, e.g., [3, 28, 44, 45]) extensions.

The main difficulty of systems of the form (1.1) both from the theoretical and the numerical point of view comes from the presence of nonconservative products (when $B \neq 0$). In fact, when the solution \mathbf{U} is discontinuous, which is a common feature of nonlinear hyperbolic systems, these nonconservative terms are not well defined in the distributional framework and the usual concept of weak solution cannot be used. There are several mathematical theories allowing to define the notion of weak solution for nonconservative systems; see, e.g., [18, 20, 60]. For instance, discontinuous solutions can be understood as the Borel measures as it was done in [20]; see also [41, 42]. This concept has been numerically utilized in [15, 22, 51, 53], where path-conservative finite-volume schemes were presented and applied to various nonconservative hyperbolic systems; also see the review papers [16, 54] and references therein. These schemes rely on the rigorous definition of the weak solution, which depends on the choice of a family of paths in the phase space. In this paper, we incorporate the CU schemes into the path-conservative framework and derive particularly simple – yet highly accurate and robust – PCCU scheme.

We also apply the designed PCCU scheme to two particular nonconservative hyperbolic systems. The first one is the Saint-Venant system of shallow water equations with discontinuous bottom topography. This system was originally proposed in [21] and is still widely used to model water flow in lakes, rivers, canals and coastal areas as well as in a variety of oceanographic and atmospheric science applications. The second system is the two-layer shallow water equations governing the flow of two superposed immiscible layers of shallow water fluids. This system, which models oceanographic water flows in straits and channels (see, e.g., [13, 48]), is conceptually more complicated than the single-layer Saint-Venant system since it contains nonconservative interlayer momentum exchange terms. Another difficulty in developing the PCCU schemes for these two systems is related to the numerical computation of steady-state and quasi-steady-state solutions. It is well known that a good numerical method for both the single- and two-layer shallow water equations should be able to exactly preserve still-water equilibria (“late at rest” states). Such schemes preserve a delicate balance between the flux and source terms on the discrete level and thus are called well-balanced schemes. We refer the reader to [1, 4, 5, 8–11, 13, 16, 23, 43, 51] for some well-balanced schemes for the systems of single- and two-layer shallow water equations, respectively. Well-balanced CU schemes were developed for both single- [7, 12, 31, 35] and two-layer [19, 36] shallow water equations. They, however, may fail to accurately capture the solution in certain situations as discussed and illustrated below. In this paper, we not only develop PCCU schemes for these two nonconservative systems, but also demonstrate the advantages of the PCCU schemes over their non-path-conservative predecessors.

The rest of the paper is organized as follows. In Section 2, we briefly review the CU schemes for 1D hyperbolic systems of conservation laws and reformulate the CU schemes in the form that fits the path-conservative framework well. In Section 3, we rigorously derive the PCCU schemes for general nonconservative hyperbolic systems. In Section 4, we develop well-balanced PCCU schemes and apply them to the Saint-Venant system with discontinuous bottom topography (Sect. 4.1) and two-layer shallow water equations (Sect. 4.2). Finally, in Section 5, we present several numerical examples demonstrating a superb performance of the proposed PCCU schemes.

2. CENTRAL-UPWIND SCHEMES FOR CONSERVATIVE SYSTEMS

We first consider the conservative hyperbolic system (1.2) and briefly review the semi-discrete CU scheme from [34]. To this end, we introduce a grid which, for simplicity, is assumed to be uniform, that is, we take $x_\alpha := \alpha \Delta x$, where Δx is a small spatial scale, and the corresponding finite-volume cells $C_j := [x_{j-\frac{1}{2}}, x_{j+\frac{1}{2}}]$. We assume that at certain time level t , the solution realized in terms of its cell averages,

$$\bar{\mathbf{U}}_j(t) = \frac{1}{\Delta x} \int_{C_j} \mathbf{U}(x, t) dx,$$

is available.

The solution is then evolved in time by solving the following system of ODEs:

$$\frac{d}{dt} \bar{\mathbf{U}}_j(t) = -\frac{\mathbf{H}_{j+\frac{1}{2}}(t) - \mathbf{H}_{j-\frac{1}{2}}(t)}{\Delta x}, \quad (2.1)$$

where the CU fluxes are (from here on we suppress the time-dependence of all indexed quantities in order to shorten the notation)

$$\mathbf{H}_{j+\frac{1}{2}} = \frac{a_{j+\frac{1}{2}}^+ \mathbf{F}(\mathbf{U}_{j+\frac{1}{2}}^-) - a_{j+\frac{1}{2}}^- \mathbf{F}(\mathbf{U}_{j+\frac{1}{2}}^+)}{a_{j+\frac{1}{2}}^+ - a_{j+\frac{1}{2}}^-} + \frac{a_{j+\frac{1}{2}}^+ a_{j+\frac{1}{2}}^-}{a_{j+\frac{1}{2}}^+ - a_{j+\frac{1}{2}}^-} (\mathbf{U}_{j+\frac{1}{2}}^+ - \mathbf{U}_{j+\frac{1}{2}}^-). \quad (2.2)$$

Here, $\mathbf{U}_{j+\frac{1}{2}}^\pm$ are the right/left-sided values of the piecewise polynomial reconstruction

$$\tilde{\mathbf{U}}(x) = \sum_j \mathbf{P}_j(x) \chi_{C_j}(x), \quad \mathbf{P}_j = (P_j^{(1)}, \dots, P_j^{(N)})^\top \quad (2.3)$$

where χ is a characteristic function and $P_j^{(i)}$ are polynomials of a certain degree satisfying the conservation and (formal) accuracy requirements, that is, for all j

$$\frac{1}{\Delta x} \int_{C_j} \mathbf{P}_j(x) dx = \bar{\mathbf{U}}_j$$

and

$$P_j^{(i)}(x) = U^{(i)}(x) + \mathcal{O}((\Delta x)^r), \quad x \in C_j,$$

where r is a (formal) order of accuracy and $\mathbf{U}(x) = (U^{(1)}, \dots, U^{(N)})^T$ is the exact smooth solution. Therefore,

$$\mathbf{U}_{j+\frac{1}{2}}^- = \mathbf{P}_j(x_{j+\frac{1}{2}}), \quad \mathbf{U}_{j+\frac{1}{2}}^+ = \mathbf{P}_{j+1}(x_{j+\frac{1}{2}}); \quad (2.4)$$

see Figure 1. The one-sided local speeds of propagation $a_{j+\frac{1}{2}}^\pm$ are an upper/lower bounds on the largest/smallest eigenvalues $\lambda_1 < \dots < \lambda_N$ of the Jacobian

$$A(\mathbf{U}) := \frac{\partial \mathbf{F}}{\partial \mathbf{U}}(\mathbf{U}).$$

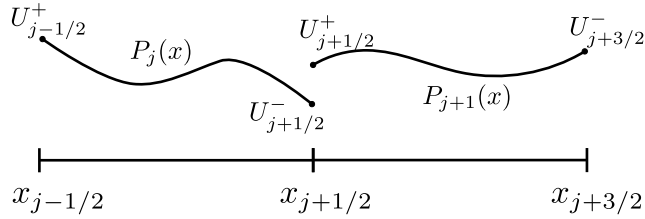


FIGURE 1. Sketch of a piecewise polynomial reconstruction.

These speeds can often be estimated by

$$\begin{aligned} a_{j+\frac{1}{2}}^- &= \min \left\{ \lambda_1(A(\mathbf{U}_{j+\frac{1}{2}}^-)), \lambda_1(A(\mathbf{U}_{j+\frac{1}{2}}^+)), 0 \right\}, \\ a_{j+\frac{1}{2}}^+ &= \max \left\{ \lambda_N(A(\mathbf{U}_{j+\frac{1}{2}}^-)), \lambda_N(A(\mathbf{U}_{j+\frac{1}{2}}^+)), 0 \right\}. \end{aligned} \quad (2.5)$$

When the analytic formulae for the largest and smallest eigenvalues are unavailable, one may obtain reasonably sharp estimates using, for example, the Lagrange theorem [39, 50]; see [36] for details on applying the Lagrange theorem in the case of the 4×4 system of two-layer shallow water equations. In Section 4.2 below, we alternatively use a first-order approximation of $a_{j+\frac{1}{2}}^-$ and $a_{j+\frac{1}{2}}^+$, which seems to be sufficiently accurate in all of the studied numerical examples.

Remark 2.1. The (formal) order of the semi-discrete CU scheme (2.1)–(2.5) is determined by the order of the piecewise polynomial reconstruction and the order of the ODE solver the system (2.1) is integrated in time.

Remark 2.2. The non-oscillatory property of the CU scheme is guaranteed provided the reconstruction (2.3) is non-oscillatory. The latter is typically achieved using nonlinear limiters; see, e.g., [46, 52, 58, 59].

Remark 2.3. We would like to point out that the first-order version of the CU scheme (2.1)–(2.5) is exactly the semi-discrete version of the HLL scheme introduced in [27].

2.1. Reformulated central-upwind scheme

We now rewrite the semi-discrete CU scheme (2.1)–(2.5). The new formulation of the scheme will then be used in Section 3 to design a PCCU scheme for the nonconservative system (1.1).

Let us define the following two coefficients:

$$\alpha_0^{j+\frac{1}{2}} := \frac{-2a_{j+\frac{1}{2}}^+ a_{j+\frac{1}{2}}^-}{a_{j+\frac{1}{2}}^+ - a_{j+\frac{1}{2}}^-}, \quad \alpha_1^{j+\frac{1}{2}} := \frac{a_{j+\frac{1}{2}}^+ + a_{j+\frac{1}{2}}^-}{a_{j+\frac{1}{2}}^+ - a_{j+\frac{1}{2}}^-},$$

using which the CU numerical flux (2.2) can be rewritten as

$$\mathbf{H}_{j+\frac{1}{2}} = \frac{1 - \alpha_1^{j+\frac{1}{2}}}{2} \mathbf{F}(\mathbf{U}_{j+\frac{1}{2}}^+) + \frac{1 + \alpha_1^{j+\frac{1}{2}}}{2} \mathbf{F}(\mathbf{U}_{j+\frac{1}{2}}^-) - \frac{\alpha_0^{j+\frac{1}{2}}}{2} (\mathbf{U}_{j+\frac{1}{2}}^+ - \mathbf{U}_{j+\frac{1}{2}}^-). \quad (2.6)$$

We then define the following two quantities:

$$\begin{aligned} \mathbf{D}_{j+\frac{1}{2}}^- &:= \mathbf{H}_{j+\frac{1}{2}} - \mathbf{F}(\mathbf{U}_{j+\frac{1}{2}}^-) = \frac{1}{2} \left[(1 - \alpha_1^{j+\frac{1}{2}}) (\mathbf{F}(\mathbf{U}_{j+\frac{1}{2}}^+) - \mathbf{F}(\mathbf{U}_{j+\frac{1}{2}}^-)) - \alpha_0^{j+\frac{1}{2}} (\mathbf{U}_{j+\frac{1}{2}}^+ - \mathbf{U}_{j+\frac{1}{2}}^-) \right], \\ \mathbf{D}_{j+\frac{1}{2}}^+ &:= \mathbf{F}(\mathbf{U}_{j+\frac{1}{2}}^+) - \mathbf{H}_{j+\frac{1}{2}} = \frac{1}{2} \left[(1 + \alpha_1^{j+\frac{1}{2}}) (\mathbf{F}(\mathbf{U}_{j+\frac{1}{2}}^+) - \mathbf{F}(\mathbf{U}_{j+\frac{1}{2}}^-)) + \alpha_0^{j+\frac{1}{2}} (\mathbf{U}_{j+\frac{1}{2}}^+ - \mathbf{U}_{j+\frac{1}{2}}^-) \right], \end{aligned} \quad (2.7)$$

which represent the differences between the numerical flux and the physical fluxes at both sides of the cell interface.

Finally, we consider a sufficiently smooth path $\Psi_{j+\frac{1}{2}}(s) := \Psi(s; \mathbf{U}_{j+\frac{1}{2}}^-, \mathbf{U}_{j+\frac{1}{2}}^+)$ connecting the states $\mathbf{U}_{j+\frac{1}{2}}^-$ and $\mathbf{U}_{j+\frac{1}{2}}^+$, that is,

$$\Psi : [0, 1] \times \mathbb{R}^N \times \mathbb{R}^N \rightarrow \mathbb{R}^N, \quad \Psi(0; \mathbf{U}_{j+\frac{1}{2}}^-, \mathbf{U}_{j+\frac{1}{2}}^+) = \mathbf{U}_{j+\frac{1}{2}}^-, \quad \Psi(1; \mathbf{U}_{j+\frac{1}{2}}^-, \mathbf{U}_{j+\frac{1}{2}}^+) = \mathbf{U}_{j+\frac{1}{2}}^+, \quad (2.8)$$

and then, equipped with (2.7), (2.8) and taking into account that

$$\mathbf{F}(\mathbf{U}_{j+\frac{1}{2}}^-) - \mathbf{F}(\mathbf{U}_{j-\frac{1}{2}}^+) = \int_{C_j} A(\mathbf{P}_j(x)) \frac{d\mathbf{P}_j}{dx} dx,$$

we rewrite the scheme (2.1), (2.6) in the following form:

$$\begin{aligned} \frac{d}{dt} \bar{\mathbf{U}}_j &= -\frac{1}{\Delta x} \left(\mathbf{H}_{j+\frac{1}{2}} - \mathbf{F}(\mathbf{U}_{j+\frac{1}{2}}^-) + \mathbf{F}(\mathbf{U}_{j-\frac{1}{2}}^+) - \mathbf{H}_{j-\frac{1}{2}} + \mathbf{F}(\mathbf{U}_{j+\frac{1}{2}}^-) - \mathbf{F}(\mathbf{U}_{j-\frac{1}{2}}^+) \right) \\ &= -\frac{1}{\Delta x} \left(\mathbf{D}_{j-\frac{1}{2}}^+ + \mathbf{D}_{j+\frac{1}{2}}^- + \int_{C_i} A(\mathbf{P}_j(x)) \frac{d\mathbf{P}_j(x)}{dx} dx \right), \end{aligned} \quad (2.9)$$

with

$$\mathbf{D}_{j+\frac{1}{2}}^\pm = \frac{1 \pm \alpha_1^{j+\frac{1}{2}}}{2} \int_0^1 A(\Psi_{j+\frac{1}{2}}(s)) \frac{d\Psi_{j+\frac{1}{2}}}{ds} ds \pm \frac{\alpha_0^{j+\frac{1}{2}}}{2} (\mathbf{U}_{j+\frac{1}{2}}^+ - \mathbf{U}_{j+\frac{1}{2}}^-). \quad (2.10)$$

3. PATH-CONSERVATIVE CENTRAL-UPWIND SCHEME

In order to design a PCCU scheme, we first rewrite the system (1.1) in the following quasilinear form:

$$\mathbf{U}_t + \mathcal{A}(\mathbf{U})\mathbf{U}_x = \mathbf{0}, \quad (3.1)$$

where

$$\mathcal{A}(\mathbf{U}) := \frac{\partial \mathbf{F}}{\partial \bar{\mathbf{U}}}(\mathbf{U}) - B(\mathbf{U}). \quad (3.2)$$

The semi-discrete scheme (2.9), (2.10) can be directly generalized to the nonconservative system (3.1), (3.2) by replacing A with \mathcal{A} :

$$\frac{d}{dt} \bar{\mathbf{U}}_j = -\frac{1}{\Delta x} \left(\mathbf{D}_{j-\frac{1}{2}}^+ + \mathbf{D}_{j+\frac{1}{2}}^- + \int_{C_i} \mathcal{A}(\mathbf{P}_j(x)) \frac{d\mathbf{P}_j(x)}{dx} dx \right), \quad (3.3)$$

where

$$\mathbf{D}_{j+\frac{1}{2}}^\pm = \frac{1 \pm \alpha_1^{j+\frac{1}{2}}}{2} \int_0^1 \mathcal{A}(\Psi_{j+\frac{1}{2}}(s)) \frac{d\Psi_{j+\frac{1}{2}}}{ds} ds \pm \frac{\alpha_0^{j+\frac{1}{2}}}{2} (\mathbf{U}_{j+\frac{1}{2}}^+ - \mathbf{U}_{j+\frac{1}{2}}^-). \quad (3.4)$$

Substituting (3.2) into (3.3) and (3.4) results in

$$\frac{d}{dt} \bar{\mathbf{U}}_j = -\frac{1}{\Delta x} \left(\mathbf{D}_{j-\frac{1}{2}}^+ + \mathbf{D}_{j+\frac{1}{2}}^- + \mathbf{F}(\mathbf{U}_{j+\frac{1}{2}}^-) - \mathbf{F}(\mathbf{U}_{j-\frac{1}{2}}^+) - \mathbf{B}_j \right), \quad (3.5)$$

where

$$\mathbf{D}_{j+\frac{1}{2}}^{\pm} = \frac{1 \pm \alpha_1^{j+\frac{1}{2}}}{2} \left(\mathbf{F}(\mathbf{U}_{j+\frac{1}{2}}^+) - \mathbf{F}(\mathbf{U}_{j+\frac{1}{2}}^-) - \mathbf{B}_{\Psi,j+\frac{1}{2}} \right) \pm \frac{\alpha_0^{j+\frac{1}{2}}}{2} \left(\mathbf{U}_{j+\frac{1}{2}}^+ - \mathbf{U}_{j+\frac{1}{2}}^- \right), \quad (3.6)$$

$$\mathbf{B}_j := \int_{C_i} B(\mathbf{P}_j(x)) \frac{d\mathbf{P}_j(x)}{dx} dx, \quad \mathbf{B}_{\Psi,j+\frac{1}{2}} := \int_0^1 B(\Psi_{j+\frac{1}{2}}(s)) \frac{d\Psi_{j+\frac{1}{2}}(s)}{ds} ds. \quad (3.7)$$

Moreover, following the same steps as in the derivation in Section 2, one may verify that (3.5)–(3.7) is equivalent to

$$\frac{d}{dt} \bar{\mathbf{U}}_j = -\frac{1}{\Delta x} \left[\mathbf{H}_{j+\frac{1}{2}} - \mathbf{H}_{j-\frac{1}{2}} - \mathbf{B}_j - \frac{a_{j-\frac{1}{2}}^+}{a_{j-\frac{1}{2}}^+ - a_{j-\frac{1}{2}}^-} \mathbf{B}_{\Psi,j-\frac{1}{2}} + \frac{a_{j+\frac{1}{2}}^-}{a_{j+\frac{1}{2}}^+ - a_{j+\frac{1}{2}}^-} \mathbf{B}_{\Psi,j+\frac{1}{2}} \right], \quad (3.8)$$

where the numerical flux $\mathbf{H}_{j+\frac{1}{2}}$ is given by the original formula (2.2).

To summarize: The *semi-discrete PCCU scheme* is given by (3.8), (2.2)–(2.5).

Remark 3.1. Notice that a straightforward discretization of the nonconservative term $B(\mathbf{U})\mathbf{U}_x$ used, for example, in [19, 29, 33, 36] leads to a very similar semi-discretization:

$$\frac{d}{dt} \bar{\mathbf{U}}_j = -\frac{1}{\Delta x} \left[\mathbf{H}_{j+\frac{1}{2}} - \mathbf{H}_{j-\frac{1}{2}} - \mathbf{B}_j \right]. \quad (3.9)$$

The only difference between (3.8) and (3.9) are the two terms

$$-\frac{a_{j-\frac{1}{2}}^+}{a_{j-\frac{1}{2}}^+ - a_{j-\frac{1}{2}}^-} \mathbf{B}_{\Psi,j-\frac{1}{2}} \quad \text{and} \quad \frac{a_{j+\frac{1}{2}}^-}{a_{j+\frac{1}{2}}^+ - a_{j+\frac{1}{2}}^-} \mathbf{B}_{\Psi,j+\frac{1}{2}},$$

which account for the contribution of the jumps of the nonconservative products at the cell interfaces. Note that these terms make the numerical scheme to become formally consistent with a particular definition of weak solutions. If those terms are neglected, as in the original CU scheme, the resulting method is only consistent with smooth solutions. We want to stress that those terms play an important role in the robustness of the numerical method as we will show in the numerical examples reported in Section 5, where the PCCU scheme clearly outperforms the original CU one.

Remark 3.2. As in the case of conservative systems, the first-order version of the PCCU scheme coincides with the semi-discrete HLL scheme for nonconservative systems; see, e.g., [16].

Remark 3.3. It is clear that the concept of weak solution and the definition of path-conservative schemes strongly depends on the chosen family of paths, which is a priori arbitrary. The crucial question is thus how to choose the “good” family of paths. The answer on this question is not easy and it is not in the scope of this paper. We refer to [16] for a detailed discussion on the subject. In this paper, we consider the canonical path which is the *segment path*.

Remark 3.4. In [15], a negative result of convergence for path-conservative numerical methods was given together with several numerical examples. Later, a new example was given in [2]. These results have led in many cases to an over-simplified picture according to which these convergence difficulties are a specific drawback of path-conservative methods.

In practice, however, path-conservative numerical methods (and in particular the proposed PCCU scheme) converge with the expected order of accuracy and, under the adequate CFL condition, with the same stability

property as their conservative counterparts. The difficulty comes from the fact that the limits of numerical solutions may differ from the *correct* ones in the case of nonconservative systems as weak solutions of nonconservative systems may be defined in infinitely many ways (for different paths).

In fact, the key point in understanding the problem of convergence for nonconservative systems is the following: the limits of the numerical solutions satisfy a jump condition which is related to the *numerical viscosity* of the method and not to the physically relevant one. Of course, this phenomenon affects any numerical method in which the small scale effects (the vanishing diffusion and/or dispersion) are not taken into account, regardless of whether it is path-conservative or not. For instance, even numerical solutions computed using the first-order Godunov scheme (which is based on the physically relevant weak solutions of the Riemann problems), may fail to converge to the physically relevant solutions: this is due to the numerical viscosity introduced at the averaging step. Again, we refer to [16] for a detailed discussion.

4. WELL-BALANCED PATH-CONSERVATIVE CENTRAL-UPWIND SCHEMES

In this section, we consider a slightly different nonconservative system

$$\mathbf{U}_t + \mathbf{F}(\mathbf{U}, Z)_x = B(\mathbf{U}, Z)\mathbf{U}_x + \mathbf{S}(\mathbf{U})Z_x, \quad (4.1)$$

where $Z = Z(x)$ is a given piecewise smooth function with a finite number of discontinuities. In such a case, the right-hand side (RHS) of (4.1) may represent a geometric source term appearing, for example, in the Saint-Venant system of shallow water equations (see Sect. 4.1) or the two-layer shallow water system (see Sect. 4.2).

It is possible to apply the PCCU scheme from Section 3 to the system (4.1). To this end, we add the $(N+1)$ -st equation $Z_t = 0$ to (4.1), introduce the extended vector of unknowns $\mathbf{W} := (\mathbf{U}^\top, Z)^\top \in \mathbb{R}^{N+1}$, and rewrite the system (4.1) in the following quasilinear form:

$$\mathbf{W}_t + \left(\begin{array}{c|c} \frac{\partial \mathbf{F}}{\partial \mathbf{U}}(\mathbf{W}) - B(\mathbf{W}) & -\widehat{\mathbf{S}}(\mathbf{W}) \\ \hline 0 & 0 \end{array} \right) \mathbf{W}_x = \mathbf{0}, \quad \widehat{\mathbf{S}}(\mathbf{W}) := \mathbf{S}(\mathbf{U}) - \frac{\partial \mathbf{F}}{\partial Z}(\mathbf{W}). \quad (4.2)$$

The PCCU scheme (3.8), (2.2)–(2.5) can now be directly applied to the system (4.2). However, the resulting scheme will have two major drawbacks. First, the numerical diffusion present in the PCCU scheme will in general affect the last equation so that the computed Z will not stay time-independent. Second, the scheme will (most probably) be not well-balanced in the sense that it will not be designed to preserve steady-state solutions of (4.1).

To overcome the first of the above difficulties, we apply the PCCU scheme (written in the form (3.5)–(3.7), (2.2)–(2.5)) to the first N equations of the system (4.2) only. This results in

$$\frac{d}{dt} \bar{\mathbf{U}}_j = -\frac{1}{\Delta x} \left(\mathbf{D}_{j-\frac{1}{2}}^+ + \mathbf{D}_{j+\frac{1}{2}}^- + \mathbf{F}(\mathbf{W}_{j+\frac{1}{2}}^-) - \mathbf{F}(\mathbf{W}_{j-\frac{1}{2}}^+) - \mathbf{B}_j - \mathbf{S}_j \right), \quad (4.3)$$

where

$$\mathbf{D}_{j+\frac{1}{2}}^\pm = \frac{1 \pm \alpha_1^{j+\frac{1}{2}}}{2} \left(\mathbf{F}(\mathbf{W}_{j+\frac{1}{2}}^+) - \mathbf{F}(\mathbf{W}_{j+\frac{1}{2}}^-) - \mathbf{B}_{\Psi,j+\frac{1}{2}} - \mathbf{S}_{\Psi,j+\frac{1}{2}} \right) \pm \frac{\alpha_0^{j+\frac{1}{2}}}{2} \left(\mathbf{U}_{j+\frac{1}{2}}^+ - \mathbf{U}_{j+\frac{1}{2}}^- \right), \quad (4.4)$$

$$\mathbf{B}_j := \int_{C_i} B(\mathbf{P}_j(x)) \left(\frac{dP_j^{(1)}(x)}{dx}, \dots, \frac{dP_j^{(N)}(x)}{dx} \right)^\top dx, \quad \mathbf{S}_j := \int_{C_i} \mathbf{S}(\mathbf{P}_j(x)) \frac{dP_j^{(N+1)}(x)}{dx} dx, \quad (4.5)$$

$$\mathbf{B}_{\Psi,j+\frac{1}{2}} := \int_0^1 B(\Psi_{j+\frac{1}{2}}(s)) \left(\frac{d\Psi_{j+\frac{1}{2}}^{(1)}(s)}{ds}, \dots, \frac{d\Psi_{j+\frac{1}{2}}^{(N)}(s)}{ds} \right)^\top ds, \quad \mathbf{S}_{\Psi,j+\frac{1}{2}} := \int_0^1 \mathbf{S}(\Psi_{j+\frac{1}{2}}(s)) \frac{d\Psi_{j+\frac{1}{2}}^{(N+1)}(s)}{ds} ds. \quad (4.6)$$

Here, a piecewise polynomial reconstruction is applied to \mathbf{W} , that is, (2.3) and (2.4) are replaced with

$$\widetilde{\mathbf{W}}(x) = \sum_j \mathbf{P}_j(x) \chi_{C_j}(x), \quad \mathbf{P}_j = (P_j^{(1)}, \dots, P_j^{(N)}, P_j^{(N+1)})^\top \quad (4.7)$$

and

$$\mathbf{W}_{j+\frac{1}{2}}^- = \mathbf{P}_j(x_{j+\frac{1}{2}}), \quad \mathbf{W}_{j+\frac{1}{2}}^+ = \mathbf{P}_{j+1}(x_{j+\frac{1}{2}}), \quad (4.8)$$

respectively, a smooth path $\Psi_{j+\frac{1}{2}}(s) = (\Psi_{j+\frac{1}{2}}^{(1)}, \dots, \Psi_{j+\frac{1}{2}}^{(N)}, \Psi_{j+\frac{1}{2}}^{(N+1)})^\top := \Psi(s; \mathbf{W}_{j+\frac{1}{2}}^-, \mathbf{W}_{j+\frac{1}{2}}^+)$ now connects the states $\mathbf{W}_{j+\frac{1}{2}}^-$ and $\mathbf{W}_{j+\frac{1}{2}}^+$, that is,

$$\Psi : [0, 1] \times \mathbb{R}^{N+1} \times \mathbb{R}^{N+1} \rightarrow \mathbb{R}^{N+1}, \quad \Psi(0; \mathbf{W}_{j+\frac{1}{2}}^-, \mathbf{W}_{j+\frac{1}{2}}^+) = \mathbf{W}_{j+\frac{1}{2}}^-, \quad \Psi(1; \mathbf{W}_{j+\frac{1}{2}}^-, \mathbf{W}_{j+\frac{1}{2}}^+) = \mathbf{W}_{j+\frac{1}{2}}^+, \quad (4.9)$$

and the one-sided local speeds are still calculated using the largest (λ_N) and smallest (λ_1) eigenvalues of

$$\mathcal{A}(\mathbf{W}) = \frac{\partial \mathbf{F}}{\partial \mathbf{U}}(\mathbf{W}) - \mathbf{B}(\mathbf{W}).$$

For example, the local speeds can be estimated using

$$\begin{aligned} a_{j+\frac{1}{2}}^- &= \min \left\{ \lambda_1(\mathcal{A}(\mathbf{W}_{j+\frac{1}{2}}^-)), \lambda_1(\mathcal{A}(\mathbf{W}_{j+\frac{1}{2}}^+)), 0 \right\}, \\ a_{j+\frac{1}{2}}^+ &= \max \left\{ \lambda_N(\mathcal{A}(\mathbf{W}_{j+\frac{1}{2}}^-)), \lambda_N(\mathcal{A}(\mathbf{W}_{j+\frac{1}{2}}^+)), 0 \right\}. \end{aligned} \quad (4.10)$$

Since the obtained scheme (4.3)–(4.10) is not guaranteed to preserve steady-state solutions of (4.1), it has to be modified further. In order to construct a well-balanced PCCU scheme, we follow the idea presented in [14, 17, 55] and add an additional term to $\mathbf{D}_{j+\frac{1}{2}}^\pm$ so that (4.4) is replaced with

$$\begin{aligned} \mathbf{D}_{j+\frac{1}{2}}^\pm &= \frac{1 \pm \alpha_1^{j+\frac{1}{2}}}{2} \left(\mathbf{F}(\mathbf{W}_{j+\frac{1}{2}}^+) - \mathbf{F}(\mathbf{W}_{j+\frac{1}{2}}^-) - \mathbf{B}_{\Psi, j+\frac{1}{2}} - \mathbf{S}_{\Psi, j+\frac{1}{2}} \right) \\ &\quad \pm \frac{\alpha_0^{j+\frac{1}{2}}}{2} \left(\mathbf{U}_{j+\frac{1}{2}}^+ - \mathbf{U}_{j+\frac{1}{2}}^- - (\mathcal{A}_{j+\frac{1}{2}}^*)^{-1} \widehat{\mathbf{S}}_{\Psi, j+\frac{1}{2}} \right). \end{aligned} \quad (4.11)$$

Here, $\mathcal{A}_{j+\frac{1}{2}}$ is an approximation of the Jacobian matrix $\mathcal{A}(\mathbf{W})$ near $x = x_{j+\frac{1}{2}}$ (e.g., one may use the Roe matrix [56], but simpler strategies such as those studied in [49] may work as well), $\mathcal{A}_{j+\frac{1}{2}}^*$ is its projection onto the subset of the state space containing the steady-state solutions to be preserved (for details see [14]; for particular examples see Sects. 4.1 and 4.2), and

$$\widehat{\mathbf{S}}_{\Psi, j+\frac{1}{2}} := \int_0^1 \widehat{\mathbf{S}}(\Psi_{j+\frac{1}{2}}(s)) \frac{d\Psi_{j+\frac{1}{2}}}{ds} ds. \quad (4.12)$$

Finally, the scheme (4.3), (4.11) can be recast in the following form (compare with (3.8), (2.2)):

$$\begin{aligned} \frac{d}{dt} \overline{\mathbf{U}}_j &= -\frac{1}{\Delta x} \left[\mathbf{H}_{j+\frac{1}{2}} - \mathbf{H}_{j-\frac{1}{2}} - \mathbf{B}_j - \mathbf{S}_j \right. \\ &\quad \left. + \frac{a_{j+\frac{1}{2}}^-}{a_{j+\frac{1}{2}}^+ - a_{j+\frac{1}{2}}^-} \left(\mathbf{B}_{\Psi, j+\frac{1}{2}} + \mathbf{S}_{\Psi, j+\frac{1}{2}} \right) - \frac{a_{j-\frac{1}{2}}^+}{a_{j-\frac{1}{2}}^+ - a_{j-\frac{1}{2}}^-} \left(\mathbf{B}_{\Psi, j-\frac{1}{2}} + \mathbf{S}_{\Psi, j-\frac{1}{2}} \right) \right], \end{aligned} \quad (4.13)$$

where the numerical flux $\mathbf{H}_{j+\frac{1}{2}}$ is given by

$$\mathbf{H}_{j+\frac{1}{2}} = \frac{a_{j+\frac{1}{2}}^+ \mathbf{F}(\mathbf{W}_{j+\frac{1}{2}}^-) - a_{j+\frac{1}{2}}^- \mathbf{F}(\mathbf{W}_{j+\frac{1}{2}}^+)}{a_{j+\frac{1}{2}}^+ - a_{j+\frac{1}{2}}^-} + \frac{a_{j+\frac{1}{2}}^+ a_{j+\frac{1}{2}}^-}{a_{j+\frac{1}{2}}^+ - a_{j+\frac{1}{2}}^-} \left(\mathbf{U}_{j+\frac{1}{2}}^+ - \mathbf{U}_{j+\frac{1}{2}}^- - (\mathcal{A}_{j+\frac{1}{2}}^*)^{-1} \widehat{\mathbf{S}}_{\Psi, j+\frac{1}{2}} \right). \quad (4.14)$$

Remark 4.1. Notice that if the original CU flux,

$$\mathbf{H}_{j+\frac{1}{2}} = \frac{a_{j+\frac{1}{2}}^+ \mathbf{F}(\mathbf{W}_{j+\frac{1}{2}}^-) - a_{j+\frac{1}{2}}^- \mathbf{F}(\mathbf{W}_{j+\frac{1}{2}}^+)}{a_{j+\frac{1}{2}}^+ - a_{j+\frac{1}{2}}^-} + \frac{a_{j+\frac{1}{2}}^+ a_{j+\frac{1}{2}}^-}{a_{j+\frac{1}{2}}^+ - a_{j+\frac{1}{2}}^-} \left(\mathbf{U}_{j+\frac{1}{2}}^+ - \mathbf{U}_{j+\frac{1}{2}}^- \right), \quad (4.15)$$

is used instead of the modified flux given by (4.14), then the scheme will be well-balanced only in the case when

$$\mathbf{U}_{j+\frac{1}{2}}^+ - \mathbf{U}_{j+\frac{1}{2}}^- \equiv \mathbf{0} \quad \text{for all } j$$

at steady states. However, in a generic case, $\mathbf{U}_{j+\frac{1}{2}}^+ - \mathbf{U}_{j+\frac{1}{2}}^-$ does not necessarily vanish, while the corresponding term appearing on the RHS of (4.14),

$$\mathbf{U}_{j+\frac{1}{2}}^+ - \mathbf{U}_{j+\frac{1}{2}}^- - (\mathcal{A}_{j+\frac{1}{2}}^*)^{-1} \widehat{\mathbf{S}}_{\Psi, j+\frac{1}{2}},$$

is in fact an approximation of $\Delta x (\mathbf{U}_x - \mathcal{A}(\mathbf{W})^{-1} \widehat{\mathbf{S}}(\mathbf{W}) Z_x)$ across the cell interface and it vanishes at steady-state solutions if a proper path is selected in the evaluation $\widehat{\mathbf{S}}_{\Psi, j+\frac{1}{2}}$ in (4.12); see [14, 17, 55] for details. This guarantees a perfect balance between the source and flux terms as long as the reconstruction (2.4) preserves the steady-state solution.

Remark 4.2. Also notice that the term we have added to make the scheme well-balanced appears in the numerical viscosity and thus does not affect the consistency of the resulting PCCU scheme (4.13), (4.14), (4.6)–(4.10).

Remark 4.3. There is a direct relation between the chosen path and the well-balanced property of path-conservative schemes. More precisely, the numerical method discussed here is well-balanced if the family of paths and the matrix $\mathcal{A}_{j+\frac{1}{2}}^*$ are such that

$$\mathcal{A}_{j+\frac{1}{2}}^* (\mathbf{U}_{j+\frac{1}{2}}^+ - \mathbf{U}_{j+\frac{1}{2}}^-) = \widehat{\mathbf{S}}_{\Psi, j+\frac{1}{2}} \quad (4.16)$$

whenever $\mathbf{U}_{j+\frac{1}{2}}^\pm$ are steady states. We note that choosing the segments path for the single- and two-layer shallow-water systems is enough to ensure that (4.16) is satisfied for “lake at rest” solutions (due to the fact that they are defined by linear relations), but a more sophisticated family of paths would be required to preserve moving-water equilibria. We refer the reader to [16] for a detailed discussion on this subject.

4.1. Application to the Saint-Venant system

We now consider a particular example of the nonconservative system (4.1) – the Saint-Venant system of shallow water equations,

$$\begin{cases} h_t + q_x = 0, \\ q_t + \left(hu^2 + \frac{g}{2} h^2 \right)_x = -ghZ_x, \end{cases} \quad (4.17)$$

where $h(x, t)$, $q(x, t)$ and $u(x, t) = q(x, t)/h(x, t)$ denote the water depth, discharge and velocity, respectively, $Z(x)$ represents the bottom topography which is assumed to be discontinuous at a finite number of points,

and g is the constant gravitational acceleration. Clearly, the system (4.17) can be written in the vector form (4.2) with $\mathbf{U} = (h, q)^\top$, $\mathbf{W} = (h, q, Z)^\top$, $\mathbf{F}(\mathbf{W}) = (q, \frac{q^2}{h} + \frac{g}{2}h^2)^\top$, $B(\mathbf{W}) \equiv 0$, and the geometric source term $\mathbf{S}(\mathbf{U}) = (0, -gh)^\top$.

In this section, we restrict our consideration to the second-order schemes, that is, the polynomial pieces in (4.7) are taken to be linear:

$$\mathbf{P}_j(x) = \overline{\mathbf{W}}_j + (\mathbf{W}_x)_j(x - x_j), \quad (4.18)$$

where $(\mathbf{W}_x)_j$ are numerical derivatives computed using a nonlinear limiter, say, using the minmod one [46, 52, 59]:

$$(\mathbf{W}_x)_j = \text{minmod}\left(\frac{\overline{\mathbf{W}}_{j+1} - \overline{\mathbf{W}}_j}{\Delta x}, \frac{\overline{\mathbf{W}}_j - \overline{\mathbf{W}}_{j-1}}{\Delta x}\right),$$

where the minmod function

$$\text{minmod}(\alpha, \beta) = \frac{\text{sgn}(\alpha) + \text{sgn}(\beta)}{2} \min(|\alpha|, |\beta|)$$

is applied to the above vector quantities in a componentwise manner.

We also take a particular example of the simplest linear segment path

$$\Psi_{j+\frac{1}{2}}(s) = \mathbf{W}_{j+\frac{1}{2}}^- + s \left(\mathbf{W}_{j+\frac{1}{2}}^+ - \mathbf{W}_{j+\frac{1}{2}}^- \right), \quad (4.19)$$

which leads to the following expressions for \mathbf{S}_j and $\mathbf{S}_{\Psi, j+\frac{1}{2}}$ in (4.5) and (4.6), respectively:

$$\mathbf{S}_j = \begin{pmatrix} 0 \\ -\frac{g}{2}(h_{j+\frac{1}{2}}^- + h_{j-\frac{1}{2}}^+)(Z_{j+\frac{1}{2}}^- - Z_{j-\frac{1}{2}}^+) \end{pmatrix}, \quad \mathbf{S}_{\Psi, j+\frac{1}{2}} = \begin{pmatrix} 0 \\ -\frac{g}{2}(h_{j+\frac{1}{2}}^+ + h_{j+\frac{1}{2}}^-)(Z_{j+\frac{1}{2}}^+ - Z_{j+\frac{1}{2}}^-) \end{pmatrix}. \quad (4.20)$$

Note that in this example, $\partial \mathbf{F} / \partial Z \equiv \mathbf{0}$ and thus $\widehat{\mathbf{S}}_{\Psi, j+\frac{1}{2}} = \mathbf{S}_{\Psi, j+\frac{1}{2}}$.

In order to design the scheme (4.13), (4.14) for the Saint-Venant system (4.17), we use its Jacobian,

$$\frac{\partial \mathbf{F}}{\partial \mathbf{U}}(\mathbf{W}) = \begin{pmatrix} 0 & 1 \\ gh - u^2 & 2u \end{pmatrix},$$

and since in this example, $\mathcal{A} = \partial \mathbf{F} / \partial \mathbf{U}$, the one-sided local speeds (4.10) are

$$\begin{aligned} a_{j+\frac{1}{2}}^- &= \min \left\{ u_{j+\frac{1}{2}}^- - \sqrt{gh_{j+\frac{1}{2}}^-}, u_{j+\frac{1}{2}}^+ - \sqrt{gh_{j+\frac{1}{2}}^+}, 0 \right\}, \\ a_{j+\frac{1}{2}}^+ &= \max \left\{ u_{j+\frac{1}{2}}^- + \sqrt{gh_{j+\frac{1}{2}}^-}, u_{j+\frac{1}{2}}^+ + \sqrt{gh_{j+\frac{1}{2}}^+}, 0 \right\}, \end{aligned} \quad (4.21)$$

and the matrices $\mathcal{A}_{j+\frac{1}{2}}^*$ and $(\mathcal{A}_{j+\frac{1}{2}}^*)^{-1}$, needed to evaluate the numerical flux (4.14), are

$$\mathcal{A}_{j+\frac{1}{2}}^* = \begin{pmatrix} 0 & 1 \\ \frac{g}{2}(h_{j+\frac{1}{2}}^+ + h_{j+\frac{1}{2}}^-) & 0 \end{pmatrix} \quad \text{and} \quad (\mathcal{A}_{j+\frac{1}{2}}^*)^{-1} = \begin{pmatrix} 2 \\ g(h_{j+\frac{1}{2}}^+ + h_{j+\frac{1}{2}}^-) \\ 1 \end{pmatrix}. \quad (4.22)$$

Note that $\mathcal{A}_{j+\frac{1}{2}}^*$ was obtained by the evaluation of $\mathcal{A}(\mathbf{W})$ at $(\mathbf{W}_{j+\frac{1}{2}}^+ + \mathbf{W}_{j+\frac{1}{2}}^-)/2$ followed by its projection onto the “lake at rest” steady state at which

$$u \equiv 0 \quad \text{and} \quad h + Z \equiv \text{Const.} \quad (4.23)$$

The resulting semi-discrete second-order PCCU scheme for the Saint-Venant system is then (4.13), (4.14) with (4.8), (4.18), (4.20)–(4.22). In order to verify that the scheme is well-balanced, we need to check whether

the last term on the RHS of (4.14) vanishes at the “lake at rest” data (4.23). Indeed, using (4.20) and (4.22) and the fact that in this example $\widehat{\mathbf{S}}_{\Psi,j+\frac{1}{2}} = \mathbf{S}_{\Psi,j+\frac{1}{2}}$, we obtain

$$\mathbf{U}_{j+\frac{1}{2}}^+ - \mathbf{U}_{j+\frac{1}{2}}^- - (\mathcal{A}_{j+\frac{1}{2}}^*)^{-1} \widehat{\mathbf{S}}_{\Psi,j+\frac{1}{2}} = \begin{pmatrix} (h_{j+\frac{1}{2}}^+ + Z_{j+\frac{1}{2}}^+) - (h_{j+\frac{1}{2}}^- + Z_{j+\frac{1}{2}}^-) \\ q_{j+\frac{1}{2}}^+ - q_{j+\frac{1}{2}}^- \end{pmatrix}. \quad (4.24)$$

Clearly, if $\bar{q}_j \equiv 0$ then all of the reconstructed values of q are zero and the second component in (4.24) vanishes. However, the first component will necessarily vanish only if we modify the piecewise linear reconstruction procedure as follows. Instead of reconstructing h , q and Z , we reconstruct $\omega := h + Z$, q and Z and then recompute

$$h_{j+\frac{1}{2}}^\pm := \omega_{j+\frac{1}{2}}^\pm - Z_{j+\frac{1}{2}}^\pm.$$

Notice that the water surface variable ω is constant at the “lake at rest” steady state (4.23) and thus all of its point values at cell interfaces will be equal and the first component in (4.24) will then vanish.

After we have ensured that the last term on the RHS of (4.14), a straightforward computation shows that at the “lake at rest” steady state (4.23), the RHS of (4.13) is equal to zero so that the resulting scheme is indeed well-balanced.

4.2. Application to the two-layer shallow water equations

We now consider another example of the nonconservative system – the two-layer shallow water system written in the same form as in [36]:

$$\begin{cases} (h_1)_t + (q_1)_x = 0, \\ (q_1)_t + \left(\frac{q_1^2}{h_1} + g\varepsilon h_1 \right)_x = g\varepsilon(h_1)_x, \\ \omega_t + (q_2)_x = 0, \\ (q_2)_t + \left(\frac{q_2^2}{\omega - Z} + \frac{g}{2} [\omega^2 - rh_1^2] - g\widehat{\varepsilon}Z \right)_x = -gr\varepsilon(h_1)_x - g\widehat{\varepsilon}Z_x. \end{cases} \quad (4.25)$$

Here, $h_1(x, t)$ and $h_2(x, t)$ are the depths of the upper (lighter) and lower (heavier) water layer of the constant densities ρ_1 and ρ_2 , respectively, $q_1(x, t)$ and $q_2(x, t)$ are the corresponding discharges, $r := \rho_1/\rho_2 \leq 1$ is the density ratio, g is the constant gravitational acceleration, $Z(x)$ represents the time-independent bottom topography, $\omega(x, t) := h_2(x, t) + Z(x)$, $\varepsilon(x, t) := h_1(x, t) + \omega(x, t)$, and $\widehat{\varepsilon}(x, t) := rh_1(x, t) + \omega(x, t)$.

Similarly to the single layer case discussed in Section 4.1, we add the fifth equation $Z_t = 0$ to the system (4.25) and rewrite it in the vector form (4.2) with $\mathbf{U} = (h_1, q_1, \omega, q_2)^T$, $\mathbf{W} = (h_1, q_1, \omega, q_2, Z)^T$, $\mathbf{F}(\mathbf{W}) = (q_1, \frac{q_1^2}{h_1} + g(h_1 + \omega)h_1, q_2, \frac{q_2^2}{\omega - Z} + \frac{g}{2} [\omega^2 - rh_1^2] - g(rh_1 + \omega)Z)^T$, and

$$B(\mathbf{W}) = \begin{pmatrix} 0 & 0 & 0 & 0 \\ g(h_1 + \omega) & 0 & 0 & 0 \\ 0 & 0 & 0 & 0 \\ -gr(h_1 + \omega) & 0 & 0 & 0 \end{pmatrix}, \quad \mathbf{S}(\mathbf{U}) = \begin{pmatrix} 0 \\ 0 \\ 0 \\ -g(rh_1 + \omega) \end{pmatrix}.$$

Notice that at the “lake at rest” steady states,

$$q_1 \equiv q_2 \equiv 0, \quad h_1 \equiv \text{Const}, \quad \omega = h_2 + Z \equiv \text{Const}, \quad (4.26)$$

that is, $\mathbf{U} \equiv \mathbf{Const}$, and thus

$$\mathbf{U}_{j+\frac{1}{2}}^+ - \mathbf{U}_{j+\frac{1}{2}}^- \equiv \mathbf{0} \quad \forall j,$$

provided the piecewise polynomial reconstruction (2.3) exactly recovers the constant states (4.26). Therefore, a well-balanced CU scheme will be obtained with the help of the original CU flux (4.15). Unfortunately, in presence of shocks, the original CU scheme is sensitive to the value ε . As a consequence, it may produce different solutions depending on the reference level or the order of the method, and it may produce strong spurious oscillations for time-dependent problems, as we demonstrate in the numerical simulations reported in Section 5.

In order to avoid the aforementioned drawbacks, the PCCU scheme (4.13), (4.15), (4.5)–(4.10) will be applied to the two-layer shallow-water system in a straightforward manner.

As in the case of a single layer, we use the piecewise linear reconstruction (4.18), which leads to the following expressions for \mathbf{B}_j and \mathbf{S}_j :

$$\mathbf{B}_j = \begin{pmatrix} 0 \\ g((\bar{h}_1)_j + \bar{\omega}_j)((h_1)_{j+\frac{1}{2}}^- - (h_1)_{j-\frac{1}{2}}^+) \\ 0 \\ -gr((\bar{h}_1)_j + \bar{\omega}_j)((h_1)_{j+\frac{1}{2}}^- - (h_1)_{j-\frac{1}{2}}^+) \end{pmatrix}, \quad \mathbf{S}_j = \begin{pmatrix} 0 \\ 0 \\ 0 \\ -g(r(\bar{h}_1)_j + \bar{\omega}_j)(Z_{j+\frac{1}{2}}^- - Z_{j-\frac{1}{2}}^+) \end{pmatrix}, \quad (4.27)$$

and the linear segment path (4.19), which results in

$$\mathbf{B}_{\Psi,j+\frac{1}{2}} = \begin{pmatrix} 0 \\ \frac{g}{2}((h_1)_{j+\frac{1}{2}}^+ + \omega_{j+\frac{1}{2}}^+ + (h_1)_{j+\frac{1}{2}}^- + \omega_{j+\frac{1}{2}}^-)((h_1)_{j+\frac{1}{2}}^+ - (h_1)_{j+\frac{1}{2}}^-) \\ 0 \\ -\frac{gr}{2}((h_1)_{j+\frac{1}{2}}^+ + \omega_{j+\frac{1}{2}}^+ + (h_1)_{j+\frac{1}{2}}^- + \omega_{j+\frac{1}{2}}^-)((h_1)_{j+\frac{1}{2}}^+ - (h_1)_{j+\frac{1}{2}}^-) \end{pmatrix} \quad (4.28)$$

and

$$\mathbf{S}_{\Psi,j+\frac{1}{2}} = \begin{pmatrix} 0 \\ 0 \\ 0 \\ -\frac{g}{2}(r(h_1)_{j+\frac{1}{2}}^+ + \omega_{j+\frac{1}{2}}^+ + r(h_1)_{j+\frac{1}{2}}^- + \omega_{j+\frac{1}{2}}^-)(Z_{j+\frac{1}{2}}^+ - Z_{j+\frac{1}{2}}^-) \end{pmatrix}. \quad (4.29)$$

In order to design the scheme (4.13), (4.14) for the two-layer system (4.25), we use the matrix

$$\mathcal{A}(\mathbf{W}) = \frac{\partial \mathbf{F}}{\partial \mathbf{U}}(\mathbf{W}) - \mathbf{B}(\mathbf{W}) = \begin{pmatrix} 0 & 1 & 0 & 0 \\ gh_1 - u_1^2 & 2u_1 & gh_1 & 0 \\ 0 & 0 & 0 & 1 \\ grh_2 & 0 & gh_2 - u_2^2 & 2u_2 \end{pmatrix}, \quad (4.30)$$

where $u_1 = q_1/h_1$, $u_2 = q_2/h_2$ and $h_2 = \omega - Z$. Then, the one-sided local speeds (4.10) are obtained using the first-order (in $u_1 - u_2$ and $(1 - r)$) approximation of the largest and smallest eigenvalues of $\mathcal{A}(\mathbf{W})$, obtained in [57]:

$$\begin{aligned} a_{j+\frac{1}{2}}^- &= \min \left\{ (u_m)_{j+\frac{1}{2}}^- - \sqrt{g((h_1)_{j+\frac{1}{2}}^- + (h_2)_{j+\frac{1}{2}}^-)}, (u_m)_{j+\frac{1}{2}}^+ - \sqrt{g((h_1)_{j+\frac{1}{2}}^+ + (h_2)_{j+\frac{1}{2}}^+)}, 0 \right\}, \\ a_{j+\frac{1}{2}}^+ &= \max \left\{ (u_m)_{j+\frac{1}{2}}^- + \sqrt{g((h_1)_{j+\frac{1}{2}}^- + (h_2)_{j+\frac{1}{2}}^-)}, (u_m)_{j+\frac{1}{2}}^+ + \sqrt{g((h_1)_{j+\frac{1}{2}}^+ + (h_2)_{j+\frac{1}{2}}^+)}, 0 \right\}, \end{aligned} \quad (4.31)$$

where $u_m := (q_1 + q_2)/(h_1 + h_2)$.

Remark 4.4. Alternatively, $a_{j+\frac{1}{2}}^\pm$ can be computed using the upper/lower bounds on the largest/smallest eigenvalues of $\mathcal{A}(\mathbf{W})$, as it was proposed in [36].

To summarize, the resulting semi-discrete second-order PCCU scheme for the two-layer shallow water system (4.25) is (4.13), (4.15) with (4.8), (4.18), (4.27)–(4.31).

4.2.1. Classical formulation of the two-layer shallow water system

We now consider a classical formulation of the two-layer shallow water system,

$$\begin{cases} (h_1)_t + (q_1)_x = 0, \\ (q_1)_t + \left(\frac{q_1^2}{h_1} + \frac{g}{2} h_1^2 \right)_x = -gh_1(h_2 + Z)_x, \\ (h_2)_t + (q_2)_x = 0, \\ (q_2)_t + \left(\frac{q_2^2}{h_2} + \frac{g}{2} h_2^2 \right)_x = -gh_2(rh_1 + Z)_x, \end{cases} \quad (4.32)$$

for which a direct application of the original CU scheme from [34] or [32] may be problematic (see [36] for details). Our goal is to show that thanks to the rigorous treatment of the nonconservative product term, the PCCU scheme can be developed and successfully applied to either formulation of the two-layer shallow water system. This will give another evidence of the robustness of the proposed PCCU approach.

Once again, we add the fifth equation $Z_t = 0$ to the system (4.32) and rewrite it in the vector form (4.2) with $\mathbf{U} = (h_1, q_1, h_2, q_2)^\top$, $\mathbf{W} = (h_1, q_1, h_2, q_2, Z)^\top$, $\mathbf{F}(\mathbf{W}) = (q_1, \frac{q_1^2}{h_1} + \frac{g}{2} h_1^2, q_2, \frac{q_2^2}{h_2} + \frac{g}{2} h_2^2)^\top$, $\partial\mathbf{F}/\partial Z \equiv \mathbf{0}$, and

$$B(\mathbf{W}) = \begin{pmatrix} 0 & 0 & 0 & 0 \\ 0 & 0 & -gh_1 & 0 \\ 0 & 0 & 0 & 0 \\ -grh_2 & 0 & 0 & 0 \end{pmatrix}, \quad \mathbf{S}(\mathbf{U}) = \begin{pmatrix} 0 \\ -gh_1 \\ 0 \\ -gh_2 \end{pmatrix}.$$

In order to apply the PCCU scheme (4.13), (4.15), (4.5)–(4.10) to the classical formulation of the two-layer shallow water system, we note that one-sided local speeds can be still computed using (4.31), and thus we only need to evaluate \mathbf{B}_j , \mathbf{S}_j , $\mathbf{B}_{\Psi,j+\frac{1}{2}}$, $\mathbf{S}_{\Psi,j+\frac{1}{2}}$, and the well-balancing term in (4.11), $\mathbf{U}_{j+\frac{1}{2}}^+ - \mathbf{U}_{j+\frac{1}{2}}^- - (\mathcal{A}_{j+\frac{1}{2}}^*)^{-1} \mathbf{S}_{\Psi,j+\frac{1}{2}}$.

As in the previous cases, we use the piecewise linear reconstruction (4.18), which leads to the following expressions for \mathbf{B}_j and \mathbf{S}_j :

$$\mathbf{B}_j = \begin{pmatrix} 0 \\ -g(\bar{h}_1)_j((h_2)_{j+\frac{1}{2}}^- - (h_2)_{j-\frac{1}{2}}^+) \\ 0 \\ -gr(\bar{h}_2)_j((h_1)_{j+\frac{1}{2}}^- - (h_1)_{j-\frac{1}{2}}^+) \end{pmatrix}, \quad \mathbf{S}_j = \begin{pmatrix} 0 \\ -g(\bar{h}_1)_j(Z_{j+\frac{1}{2}}^- - Z_{j-\frac{1}{2}}^+) \\ 0 \\ -g(\bar{h}_2)_j(Z_{j+\frac{1}{2}}^- - Z_{j-\frac{1}{2}}^+) \end{pmatrix}, \quad (4.33)$$

and the linear segment path (4.19), which results in

$$\mathbf{B}_{\Psi,j+\frac{1}{2}} = \begin{pmatrix} 0 \\ -\frac{g}{2}((h_1)_{j+\frac{1}{2}}^+ + (h_1)_{j+\frac{1}{2}}^-)((h_2)_{j+\frac{1}{2}}^+ - (h_2)_{j+\frac{1}{2}}^-) \\ 0 \\ -\frac{gr}{2}((h_2)_{j+\frac{1}{2}}^+ + (h_2)_{j+\frac{1}{2}}^-)((h_1)_{j+\frac{1}{2}}^+ - (h_1)_{j+\frac{1}{2}}^-) \end{pmatrix} \quad (4.34)$$

and

$$\mathbf{S}_{\Psi,j+\frac{1}{2}} = \begin{pmatrix} 0 \\ -\frac{g}{2}((h_1)_{j+\frac{1}{2}}^+ + (h_1)_{j+\frac{1}{2}}^-)(Z_{j+\frac{1}{2}}^+ - Z_{j+\frac{1}{2}}^-) \\ 0 \\ -\frac{g}{2}((h_2)_{j+\frac{1}{2}}^+ + (h_2)_{j+\frac{1}{2}}^-)(Z_{j+\frac{1}{2}}^+ - Z_{j+\frac{1}{2}}^-) \end{pmatrix}. \quad (4.35)$$

Finally, the matrices $A_{j+\frac{1}{2}}^*$ and $(A_{j+\frac{1}{2}}^*)^{-1}$, needed to evaluate the numerical flux (4.14), are

$$\mathcal{A}_{j+\frac{1}{2}}^* = \begin{pmatrix} 0 & 1 & 0 & 0 \\ \frac{g}{2}((h_1)_{j+\frac{1}{2}}^+ + (h_1)_{j+\frac{1}{2}}^-) & 0 & \frac{g}{2}((h_1)_{j+\frac{1}{2}}^+ + (h_1)_{j+\frac{1}{2}}^-) & 0 \\ 0 & 0 & 0 & 1 \\ \frac{gr}{2}((h_2)_{j+\frac{1}{2}}^+ + (h_2)_{j+\frac{1}{2}}^-) & 0 & \frac{g}{2}((h_2)_{j+\frac{1}{2}}^+ + (h_2)_{j+\frac{1}{2}}^-) & 0 \end{pmatrix} \quad (4.36)$$

and

$$(\mathcal{A}_{j+\frac{1}{2}}^*)^{-1} = \begin{pmatrix} 0 & 2 & 0 & 2 \\ 0 & g(1-r)((h_1)_{j+\frac{1}{2}}^+ + (h_1)_{j+\frac{1}{2}}^-) & 0 & g(r-1)((h_2)_{j+\frac{1}{2}}^+ + (h_2)_{j+\frac{1}{2}}^-) \\ 1 & 0 & 0 & 0 \\ 0 & 2r & 0 & 2 \\ 0 & g(r-1)((h_1)_{j+\frac{1}{2}}^+ + (h_1)_{j+\frac{1}{2}}^-) & 0 & g(1-r)((h_2)_{j+\frac{1}{2}}^+ + (h_2)_{j+\frac{1}{2}}^-) \\ 0 & 0 & 1 & 0 \end{pmatrix}. \quad (4.37)$$

Note that $\mathcal{A}_{j+\frac{1}{2}}^*$ was obtained by the evaluation of $\mathcal{A}(\mathbf{W})$, given by (4.30), at $(\mathbf{W}_{j+\frac{1}{2}}^+ + \mathbf{W}_{j+\frac{1}{2}}^-)/2$ followed by its projection onto the “lake at rest” steady state at which $q_1 \equiv q_2 \equiv 0$.

The resulting semi-discrete second-order PCCU scheme for the two-layer shallow water system (4.32) is then given by (4.13), (4.14) with (4.8), (4.18), (4.31), (4.33)–(4.37). To verify that the scheme is well-balanced, we need to check whether the last term on the RHS of (4.14) vanishes at the “lake at rest” data (4.26). To this end, we note that now, as in the single-layer case, $\partial \mathbf{F} / \partial Z \equiv \mathbf{0}$ and thus $\hat{\mathbf{S}}_{\Psi, j+\frac{1}{2}} = \mathbf{S}_{\Psi, j+\frac{1}{2}}$. Therefore, using (4.29) and (4.37) we obtain

$$\mathbf{U}_{j+\frac{1}{2}}^+ - \mathbf{U}_{j+\frac{1}{2}}^- - (A_{j+\frac{1}{2}}^*)^{-1} \mathbf{S}_{\Psi, j+\frac{1}{2}} = \begin{pmatrix} (h_1)_{j+\frac{1}{2}}^+ - (h_1)_{j+\frac{1}{2}}^- \\ (q_1)_{j+\frac{1}{2}}^+ - (q_1)_{j+\frac{1}{2}}^- \\ ((h_2)_{j+\frac{1}{2}}^+ + Z_{j+\frac{1}{2}}^+) - ((h_2)_{j+\frac{1}{2}}^- + Z_{j+\frac{1}{2}}^-) \\ (q_2)_{j+\frac{1}{2}}^+ - (q_2)_{j+\frac{1}{2}}^- \end{pmatrix}. \quad (4.38)$$

Since at the “lake at rest” steady state $q_1 \equiv q_2 \equiv 0$ and $h_1 \equiv \text{Const}$, then all of the reconstructed values of h_1 , q_1 and q_2 are the same and the first, second and forth components in (4.38) vanish. However, the third component will necessarily vanish only if we reconstruct h_1 , q_1 , $\omega := h_2 + Z$, q_2 and Z (instead of reconstructing h_1 , q_1 , h_2 , q_2 and Z) and then recompute

$$(h_2)_{j+\frac{1}{2}}^\pm := \omega_{j+\frac{1}{2}}^\pm - Z_{j+\frac{1}{2}}^\pm.$$

Indeed, since the variable ω is constant at the “lake at rest” steady state (4.26), all of its point values at cell interfaces will be equal and the third component in (4.38) will then vanish.

After we have ensured that the last term on the RHS of (4.14), a straightforward computation shows that at the “lake at rest” steady state (4.26), the RHS of (4.13) is equal to zero so that the resulting scheme is indeed well-balanced.

4.2.2. Equivalence of path-conservative central-upwind schemes for (4.25) and (4.32)

As we have previously pointed out, the original CU scheme does not take into account the discontinuities of the nonconservative products at the cell interfaces. This fact together with the non-well-balanced nature of the original CU scheme makes it impossible to apply it to the original formulation of the two-layer shallow water system (4.32). This is the reason why a new reformulation of the two-layer shallow-water system (4.25) was proposed in [36]. When applied to this formulation, the original CU scheme is well-balanced and may produce satisfactory results if $\varepsilon \sim 0$ and no strong shocks appear. However, for discontinuous solutions, the numerical

derivative of h_1 is $\mathcal{O}(\Delta x^{-1})$, so that the product $\varepsilon(h_1)_x$ may not be small, in which case the original CU scheme may fail to produce accurate solution.

At the same time, when the PCCU scheme with the linear path is applied to these systems, the resulting schemes, (4.13), (4.15), (4.8), (4.18), (4.31), (4.27)–(4.30) for the system (4.25) and (4.13), (4.15), (4.8), (4.18), (4.31), (4.33)–(4.38) for the system (4.32), are in fact equivalent, as we are going to show in this section.

First, we note that the first equations in (4.25) and (4.32) as well as their semi-discretization are exactly the same. The third equations are not the same since the evolved quantities in (4.25) and (4.32) are ω and h_2 , respectively. However, since the bottom topography Z is time-independent and since the numerical fluxes are exactly the same, the semi-discretizations of the third equations in (4.25) and (4.32) coincide as well.

We now consider the second equations in (4.25) and (4.32). Since the evolved quantities are the same (q_1), it will be enough to show that the RHSs of the second components in the semi-discretizations (4.13) are the same for both systems. Indeed, the second component of (4.13) for the system (4.25) is

$$\begin{aligned} \text{RHS}_{(4.25)}^{(2)} = & -\frac{1}{\Delta x} \left[\frac{a_{j+\frac{1}{2}}^+ \left\{ \frac{(q_1)^2}{h_1} + gh_1(h_1 + \omega) \right\}_{j+\frac{1}{2}}^- - a_{j+\frac{1}{2}}^+ \left\{ \frac{(q_1)^2}{h_1} + gh_1(h_1 + \omega) \right\}_{j+\frac{1}{2}}^+}{a_{j+\frac{1}{2}}^+ - a_{j+\frac{1}{2}}^-} \right. \\ & + \frac{a_{j+\frac{1}{2}}^+ a_{j+\frac{1}{2}}^-}{a_{j+\frac{1}{2}}^+ - a_{j+\frac{1}{2}}^-} \left((q_1)_{j+\frac{1}{2}}^+ - (q_1)_{j+\frac{1}{2}}^- \right) - \frac{a_{j-\frac{1}{2}}^+ a_{j-\frac{1}{2}}^-}{a_{j-\frac{1}{2}}^+ - a_{j-\frac{1}{2}}^-} \left((q_1)_{j-\frac{1}{2}}^+ - (q_1)_{j-\frac{1}{2}}^- \right) \\ & - \frac{a_{j-\frac{1}{2}}^+ \left\{ \frac{(q_1)^2}{h_1} + gh_1(h_1 + \omega) \right\}_{j-\frac{1}{2}}^- - a_{j-\frac{1}{2}}^+ \left\{ \frac{(q_1)^2}{h_1} + gh_1(h_1 + \omega) \right\}_{j-\frac{1}{2}}^+}{a_{j-\frac{1}{2}}^+ - a_{j-\frac{1}{2}}^-} \\ & - g((\bar{h}_1)_j + \bar{\omega}_j)((h_1)_{j+\frac{1}{2}}^- - (h_1)_{j-\frac{1}{2}}^+) \\ & + \frac{a_{j+\frac{1}{2}}^-}{a_{j+\frac{1}{2}}^+ - a_{j+\frac{1}{2}}^-} \left\{ \frac{g}{2} \left((h_1)_{j+\frac{1}{2}}^+ + \omega_{j+\frac{1}{2}}^+ + (h_1)_{j+\frac{1}{2}}^- + \omega_{j+\frac{1}{2}}^- \right) \left((h_1)_{j+\frac{1}{2}}^+ - (h_1)_{j+\frac{1}{2}}^- \right) \right\} \\ & \left. - \frac{a_{j-\frac{1}{2}}^+}{a_{j-\frac{1}{2}}^+ - a_{j-\frac{1}{2}}^-} \left\{ \frac{g}{2} \left((h_1)_{j-\frac{1}{2}}^+ + \omega_{j-\frac{1}{2}}^+ + (h_1)_{j-\frac{1}{2}}^- + \omega_{j-\frac{1}{2}}^- \right) \left((h_1)_{j-\frac{1}{2}}^+ - (h_1)_{j-\frac{1}{2}}^- \right) \right\} \right], \end{aligned}$$

and for the system (4.32) it is equal to

$$\begin{aligned} \text{RHS}_{(4.32)}^{(2)} = & -\frac{1}{\Delta x} \left[\frac{a_{j+\frac{1}{2}}^+ \left\{ \frac{(q_1)^2}{h_1} + \frac{g}{2} h_1^2 \right\}_{j+\frac{1}{2}}^- - a_{j+\frac{1}{2}}^+ \left\{ \frac{(q_1)^2}{h_1} + \frac{g}{2} h_1^2 \right\}_{j+\frac{1}{2}}^+}{a_{j+\frac{1}{2}}^+ - a_{j+\frac{1}{2}}^-} \right. \\ & + \frac{a_{j+\frac{1}{2}}^+ a_{j+\frac{1}{2}}^-}{a_{j+\frac{1}{2}}^+ - a_{j+\frac{1}{2}}^-} \left((q_1)_{j+\frac{1}{2}}^+ - (q_1)_{j+\frac{1}{2}}^- \right) - \frac{a_{j-\frac{1}{2}}^+ a_{j-\frac{1}{2}}^-}{a_{j-\frac{1}{2}}^+ - a_{j-\frac{1}{2}}^-} \left((q_1)_{j-\frac{1}{2}}^+ - (q_1)_{j-\frac{1}{2}}^- \right) \\ & - \frac{a_{j-\frac{1}{2}}^+ \left\{ \frac{(q_1)^2}{h_1} + \frac{g}{2} h_1^2 \right\}_{j-\frac{1}{2}}^- - a_{j-\frac{1}{2}}^+ \left\{ \frac{(q_1)^2}{h_1} + \frac{g}{2} h_1^2 \right\}_{j-\frac{1}{2}}^+}{a_{j-\frac{1}{2}}^+ - a_{j-\frac{1}{2}}^-} \\ & - g(\bar{h}_1)_j (\omega_{j+\frac{1}{2}}^- - \omega_{j-\frac{1}{2}}^+) \end{aligned}$$

$$\begin{aligned}
& - \frac{a_{j+\frac{1}{2}}^-}{a_{j+\frac{1}{2}}^+ - a_{j+\frac{1}{2}}^-} \left\{ \frac{g}{2} \left((h_1)_{j+\frac{1}{2}}^+ + (h_1)_{j+\frac{1}{2}}^- \right) \left(\omega_{j+\frac{1}{2}}^+ - \omega_{j+\frac{1}{2}}^- \right) \right\} \\
& + \frac{a_{j-\frac{1}{2}}^+}{a_{j-\frac{1}{2}}^+ - a_{j-\frac{1}{2}}^-} \left\{ \frac{g}{2} \left((h_1)_{j-\frac{1}{2}}^+ + (h_1)_{j-\frac{1}{2}}^- \right) \left(\omega_{j-\frac{1}{2}}^+ - \omega_{j-\frac{1}{2}}^- \right) \right\} \Bigg].
\end{aligned}$$

A straightforward computation shows that $\text{RHS}_{(4.25)}^{(2)} = \text{RHS}_{(4.32)}^{(2)}$.

Finally, for the fourth components of (4.13) applied to the systems (4.25) and (4.32), we will obtain

$$\begin{aligned}
\text{RHS}_{(4.25)}^{(4)} = & - \frac{1}{\Delta x} \left[\frac{a_{j+\frac{1}{2}}^+ \left\{ \frac{(q_2)^2}{\omega - Z} + \frac{g}{2} [\omega^2 - rh_1^2] - g(rh_1 + \omega)Z \right\}_{j+\frac{1}{2}}^-}{a_{j+\frac{1}{2}}^+ - a_{j+\frac{1}{2}}^-} \right. \\
& - \frac{a_{j+\frac{1}{2}}^+ \left\{ \frac{(q_2)^2}{\omega - Z} + \frac{g}{2} [\omega - rh_1^2] - g(rh_1 + \omega)Z \right\}_{j+\frac{1}{2}}^+}{a_{j+\frac{1}{2}}^+ - a_{j+\frac{1}{2}}^-} \\
& + \frac{a_{j+\frac{1}{2}}^+ a_{j+\frac{1}{2}}^-}{a_{j+\frac{1}{2}}^+ - a_{j+\frac{1}{2}}^-} \left((q_2)_{j+\frac{1}{2}}^+ - (q_2)_{j+\frac{1}{2}}^- \right) - \frac{a_{j-\frac{1}{2}}^+ a_{j-\frac{1}{2}}^-}{a_{j-\frac{1}{2}}^+ - a_{j-\frac{1}{2}}^-} \left((q_2)_{j-\frac{1}{2}}^+ - (q_2)_{j-\frac{1}{2}}^- \right) \\
& - \frac{a_{j-\frac{1}{2}}^+ \left\{ \frac{(q_2)^2}{\omega - Z} + \frac{g}{2} [\omega^2 - rh_1^2] - g(rh_1 + \omega)Z \right\}_{j-\frac{1}{2}}^-}{a_{j-\frac{1}{2}}^+ - a_{j-\frac{1}{2}}^-} \\
& + \frac{a_{j-\frac{1}{2}}^+ \left\{ \frac{(q_2)^2}{\omega - Z} + \frac{g}{2} [\omega - rh_1^2] - g(rh_1 + \omega)Z \right\}_{j-\frac{1}{2}}^+}{a_{j-\frac{1}{2}}^+ - a_{j-\frac{1}{2}}^-} \\
& - gr((\bar{h}_1)_j + \bar{\omega}_j) ((h_1)_{j+\frac{1}{2}}^- - (h_1)_{j-\frac{1}{2}}^+) - g(r(\bar{h}_1)_j + \bar{\omega}_j) (Z_{j+\frac{1}{2}}^- - Z_{j-\frac{1}{2}}^+) \\
& - \frac{a_{j+\frac{1}{2}}^-}{a_{j+\frac{1}{2}}^+ - a_{j+\frac{1}{2}}^-} \left\{ \frac{gr}{2} \left((h_1)_{j+\frac{1}{2}}^+ + \omega_{j+\frac{1}{2}}^+ + (h_1)_{j+\frac{1}{2}}^- + \omega_{j+\frac{1}{2}}^- \right) \left((h_1)_{j+\frac{1}{2}}^+ - (h_1)_{j+\frac{1}{2}}^- \right) \right. \\
& + \frac{g}{2} \left(r(h_1)_{j+\frac{1}{2}}^+ + \omega_{j+\frac{1}{2}}^+ + r(h_1)_{j+\frac{1}{2}}^- + \omega_{j+\frac{1}{2}}^- \right) \left(Z_{j+\frac{1}{2}}^+ - Z_{j+\frac{1}{2}}^- \right) \Big\} \\
& + \frac{a_{j-\frac{1}{2}}^+}{a_{j-\frac{1}{2}}^+ - a_{j-\frac{1}{2}}^-} \left\{ \frac{gr}{2} \left((h_1)_{j-\frac{1}{2}}^+ + \omega_{j-\frac{1}{2}}^+ + (h_1)_{j-\frac{1}{2}}^- + \omega_{j-\frac{1}{2}}^- \right) \left((h_1)_{j-\frac{1}{2}}^+ - (h_1)_{j-\frac{1}{2}}^- \right) \right. \\
& \left. \left. + \frac{g}{2} \left(r(h_1)_{j-\frac{1}{2}}^+ + \omega_{j-\frac{1}{2}}^+ + r(h_1)_{j-\frac{1}{2}}^- + \omega_{j-\frac{1}{2}}^- \right) \left(Z_{j-\frac{1}{2}}^+ - Z_{j-\frac{1}{2}}^- \right) \right\} \right],
\end{aligned}$$

and

$$\text{RHS}_{(4.32)}^{(4)} = - \frac{1}{\Delta x} \left[\frac{a_{j+\frac{1}{2}}^+ \left\{ \frac{(q_2)^2}{\omega - Z} + \frac{g}{2} [\omega^2 - Z^2] \right\}_{j+\frac{1}{2}}^- - a_{j+\frac{1}{2}}^+ \left\{ \frac{(q_2)^2}{\omega - Z} + \frac{g}{2} [\omega - Z^2] \right\}_{j+\frac{1}{2}}^+}{a_{j+\frac{1}{2}}^+ - a_{j+\frac{1}{2}}^-} \right.$$

$$\begin{aligned}
& + \frac{a_{j+\frac{1}{2}}^+ a_{j+\frac{1}{2}}^-}{a_{j+\frac{1}{2}}^+ - a_{j+\frac{1}{2}}^-} \left((q_2)_{j+\frac{1}{2}}^+ - (q_2)_{j+\frac{1}{2}}^- \right) - \frac{a_{j-\frac{1}{2}}^+ a_{j-\frac{1}{2}}^-}{a_{j-\frac{1}{2}}^+ - a_{j-\frac{1}{2}}^-} \left((q_2)_{j-\frac{1}{2}}^+ - (q_2)_{j-\frac{1}{2}}^- \right) \\
& - \frac{a_{j-\frac{1}{2}}^+ \left\{ \frac{(q_2)^2}{\omega - Z} + \frac{g}{2} [\omega^2 - Z^2] \right\}_{j-\frac{1}{2}}^- + a_{j-\frac{1}{2}}^+ \left\{ \frac{(q_2)^2}{\omega - Z} + \frac{g}{2} [\omega - Z^2] \right\}_{j-\frac{1}{2}}^+}{a_{j-\frac{1}{2}}^+ - a_{j-\frac{1}{2}}^-} \\
& - g(\bar{h}_2)_j \left(r(h_1)_{j+\frac{1}{2}}^- + Z_{j+\frac{1}{2}}^- - r(h_1)_{j-\frac{1}{2}}^+ - Z_{j-\frac{1}{2}}^+ \right) \\
& - \frac{a_{j+\frac{1}{2}}^-}{a_{j+\frac{1}{2}}^+ - a_{j+\frac{1}{2}}^-} \left\{ \frac{g}{2} \left(\omega_{j+\frac{1}{2}}^+ - Z_{j+\frac{1}{2}}^+ + \omega_{j+\frac{1}{2}}^- - Z_{j+\frac{1}{2}}^- \right) \left(r(h_1)_{j+\frac{1}{2}}^+ + Z_{j+\frac{1}{2}}^+ - r(h_1)_{j+\frac{1}{2}}^- - Z_{j+\frac{1}{2}}^- \right) \right\} \\
& + \frac{a_{j-\frac{1}{2}}^+}{a_{j-\frac{1}{2}}^+ - a_{j-\frac{1}{2}}^-} \left\{ \frac{g}{2} \left(\omega_{j-\frac{1}{2}}^+ - Z_{j-\frac{1}{2}}^+ + \omega_{j-\frac{1}{2}}^- - Z_{j-\frac{1}{2}}^- \right) \left(r(h_1)_{j-\frac{1}{2}}^+ + Z_{j-\frac{1}{2}}^+ - r(h_1)_{j-\frac{1}{2}}^- - Z_{j-\frac{1}{2}}^- \right) \right\} \Bigg],
\end{aligned}$$

respectively, and then one can easily verify that $\text{RHS}_{(4.25)}^{(4)} = \text{RHS}_{(4.32)}^{(4)}$.

5. NUMERICAL EXAMPLES

In this section, we test the proposed PCCU scheme on a number of numerical examples and demonstrate that it outperforms the original CU scheme. We first study the single layer Saint-Venant system with discontinuous bottom topography (Sect. 5.1) and then proceed with the more complicated two-layer shallow water equations (Sect. 5.2).

In all of the numerical examples below:

- We use the constant gravitational acceleration $g = 9.81$;
- The systems of ODEs obtained as a result of the studied semi-discretizations have been integrated in time using the second-order strong stability preserving (SSP) Runge-Kutta solver (the Heun method); see, *e.g.*, [25, 26].

In Examples 5.1–5.3, we solve the initial values problems (IVPs), that is, we take sufficiently large computational domains so that the solution remains flat at the boundaries so that we can safely use zero-order extrapolation for all of the computed quantities there. In Example 5.4, a small barotropic perturbation is imposed at the left boundary of the computational domain.

5.1. Saint-Venant system with discontinuous bottom topography

Example 5.1 (Dam-Break Problem). We begin with the case of single layer shallow water equations with the following bottom topography:

$$Z(x) = \begin{cases} -0.5, & \text{if } x < 0.1 - \delta, \\ -0.5 - \frac{0.2}{\delta}(x - 0.1 + \delta), & \text{if } 0.1 - \delta \leq x \leq 0.1 + \delta, \\ -0.9, & \text{if } x > 0.1 + \delta, \end{cases}$$

where δ is a parameter that can be used to control the steepness of the slope in B .

The initial data that correspond to a dam break are given by

$$\omega(x, 0) = h(x, 0) + Z(x) = \begin{cases} 1, & \text{if } x < 0, \\ 0, & \text{if } x > 0, \end{cases} \quad q(x, 0) \equiv 0.$$

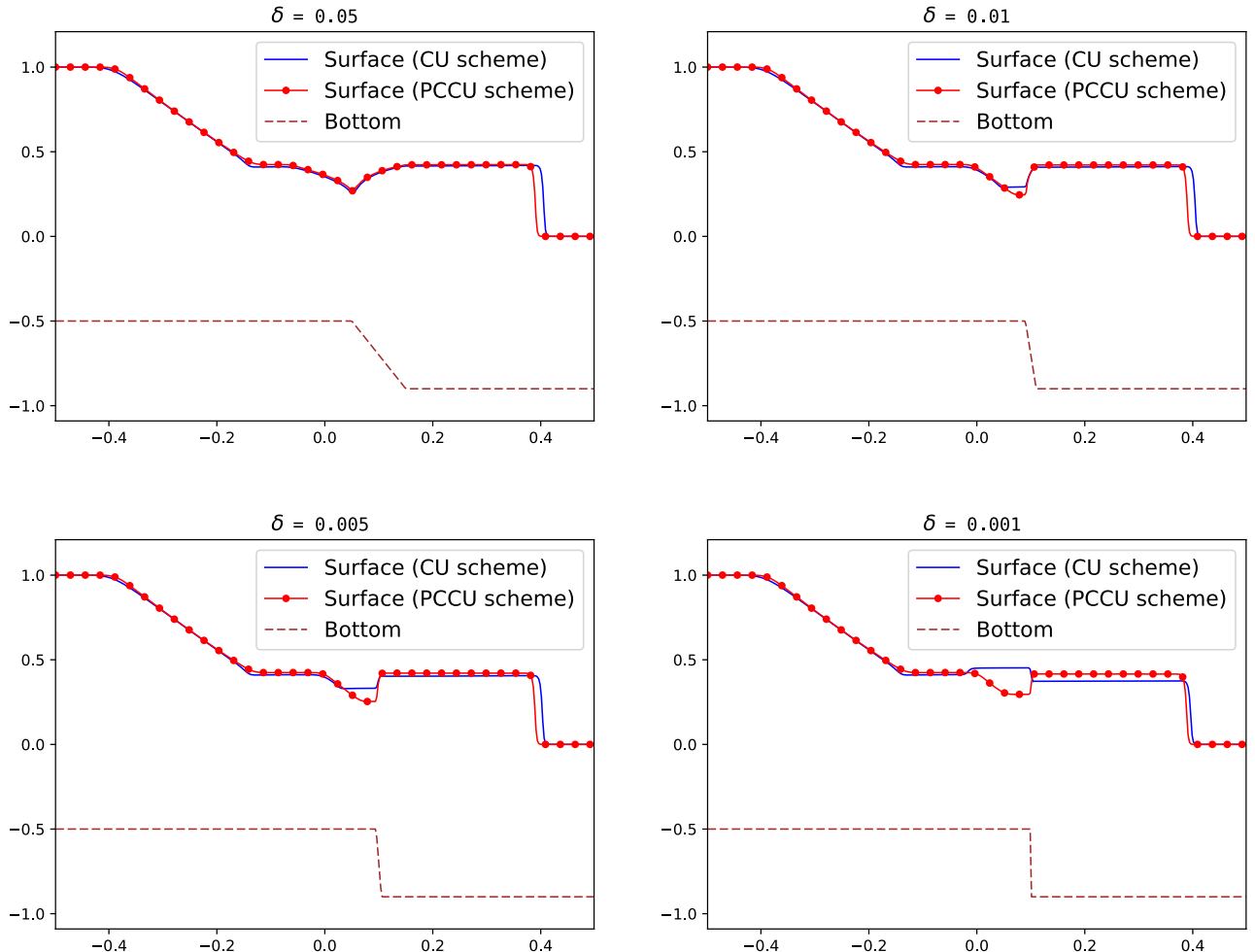


FIGURE 2. Example 5.1: water surface ω computed using the PCCU and CU schemes for four different values of $\delta = 0.05, 0.01, 0.005$ and 0.001 and the corresponding bottom topographies.

We take four different values of $\delta = 0.05, 0.01, 0.005$ and 0.001 and compute the solutions of the four corresponding IVPs at the final time $t = 0.1$ using the second-order PCCU and CU schemes on the grid with 400 uniform finite-volume cells on the computational domain $[-0.5, 0.5]$. We note that in the case of the smallest $\delta = 0.001$, the bottom topography jumps down from -0.5 to -0.9 within the interval of size $2\delta = 0.002$, which is smaller than $\Delta x = 0.0025$, that is, in this case the bottom topography can be in fact considered discontinuous for any practical purpose.

The computed solutions (water surface ω) are presented in Figure 2 together with the corresponding bottom structures. As one can clearly see, when δ is sufficiently large ($\delta = 0.05$), both PCCU and CU schemes give quite similar results. They, however, become more and more different when δ is reduced, and for the smallest $\delta = 0.001$ they are already qualitatively different.

In order to verify that the PCCU solution is the accurate one, we perform the mesh refinement study of both the PCCU and CU schemes in the case of $\delta = 0.001$. We take a sequence of uniform grids with 800, 1600 and 3200 cells and report the obtained results in Figure 3. As one can see, both schemes seem to eventually

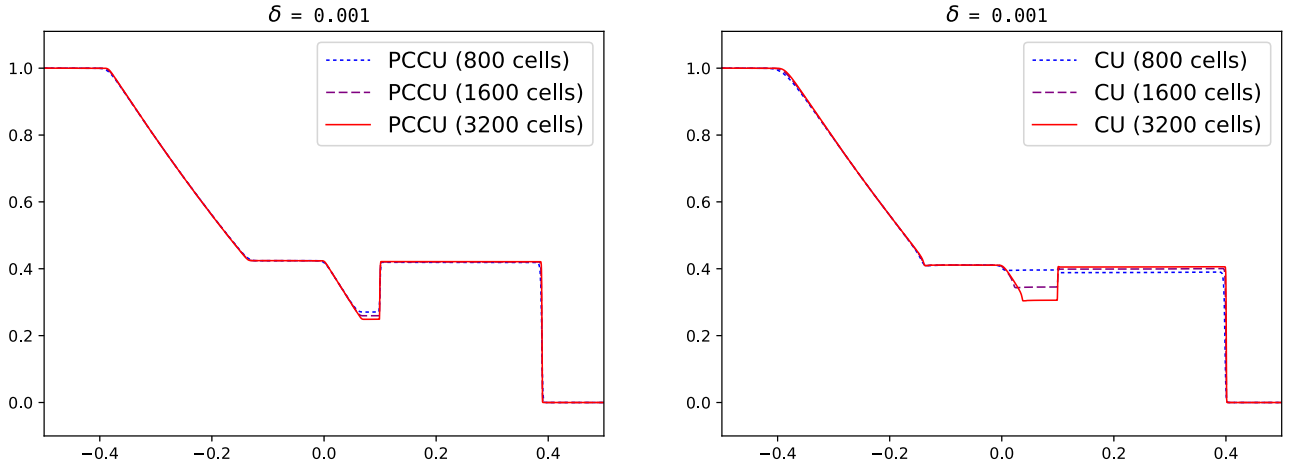


FIGURE 3. Example 5.1: water surface ω computed by the PCCU (*left panel*) and CU (*right panel*) schemes for $\delta = 0.001$ using three different grids.

converge to the same solution, but the convergence of the PCCU scheme is much faster, which confirms the high resolution and robustness of the proposed PCCU approach.

5.2. Two-layer shallow water equations

We now proceed with three examples for the two-layer shallow water equations. We restrict our consideration to the case of a flat bottom topography $Z(x) \equiv \text{Const}$ since the nonconservative interlayer exchange terms on the RHS of (4.32) introduce a more severe computational challenge than the corresponding geometric source terms.

Example 5.2 (Riemann Problem with Initially Flat Water Surface). In this example, we take $Z(x) \equiv -2$ and consider the following initial data:

$$h_1(x, 0) = \begin{cases} 1.8, & \text{if } x < 0, \\ 0.2, & \text{if } x > 0, \end{cases} \quad h_2(x, 0) = \begin{cases} 0.2, & \text{if } x < 0, \\ 1.8, & \text{if } x > 0, \end{cases} \quad q_1(x, 0) \equiv q_2(x, 0) \equiv 0.$$

Note that initially the water surface is flat since $\varepsilon(x, 0) = h_1(x, 0) + h_2(x, 0) + Z(x) \equiv 0$.

We first apply the second-order PCCU and CU schemes on the grid with 400 uniform finite-volume cells on the computational domain $[-5, 5]$. The solutions (water surface $\varepsilon = h_1 + h_2 + Z$ and interface $\omega = h_2 + Z$) computed at the final time $t = 7$ are reported in Figure 4. As we can see, both second order-schemes give similar results, although small differences can be observed.

To see an advantage of the PCCU scheme, we now compute the same solution using the first-order PCCU and CU schemes, which are obtained by using a piecewise constant reconstruction in (2.4), that is, by setting $\mathbf{U}_{j+\frac{1}{2}}^- = \bar{\mathbf{U}}_j$ and $\mathbf{U}_{j+\frac{1}{2}}^+ = \bar{\mathbf{U}}_{j+1}$. We experimentally study the convergence of these two schemes by refining the mesh and using 400, 800 and 1600 uniform cells. As one can see in Figure 5, the first-order PCCU solutions seem to approach the corresponding second-order one, which is plotted both here and in Figure 4. This is, however, not the case for the first-order CU scheme, which produces a sequence of the solutions that does not seem to approach the corresponding second-order solution as can be clearly seen in Figure 6. This provides an additional evidence of the robustness of the proposed PCCU approach.

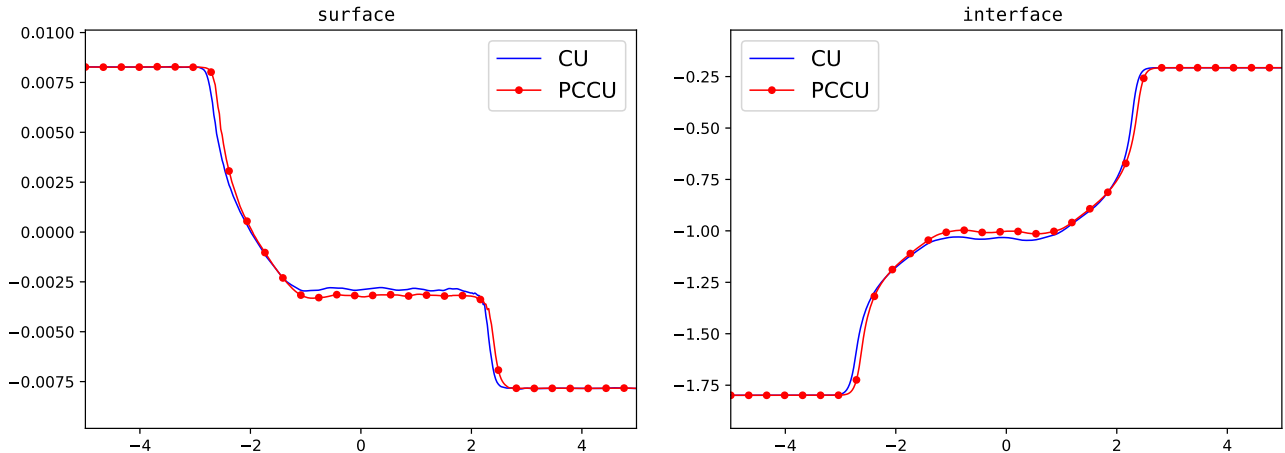


FIGURE 4. Example 5.2: water surface ε (left panel) and interface ω (right panel) computed using the second-order PCCU and CU schemes.

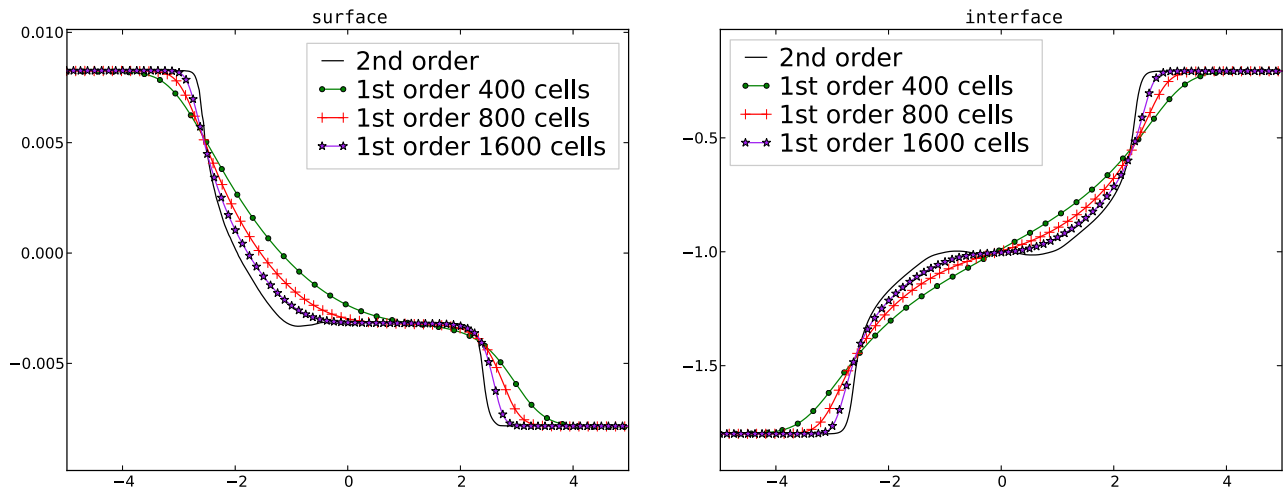


FIGURE 5. Example 5.2: experimental convergence study for the first-order PCCU scheme: Water surface ε (left panel) and interface ω (right panel) computed on three different grids. The obtained results are compared with the second-order ones.

Example 5.3 (Isolated Internal Shock). We begin by considering the following IVP: the system (4.32) with $Z(x) \equiv Z_{\text{ref}} = \text{Const}$ and the Riemann initial data

$$\mathbf{U}(x, 0) = \begin{cases} \mathbf{U}_L, & \text{if } x < 0, \\ \mathbf{U}_R, & \text{if } x > 0, \end{cases} \quad (5.1)$$

with

$$\mathbf{U}_R = ((h_1)_R, (q_1)_R, (h_2)_R, (q_2)_R)^T = (0.37002, -0.18684, 1.59310, 0.17416)^T \quad (5.2)$$

and

$$\mathbf{U}_L = ((h_1)_L, (q_1)_L, (h_2)_L, (q_2)_L)^T = (1.22582, -0.03866, 0.75325, 0.02893)^T, \quad (5.3)$$

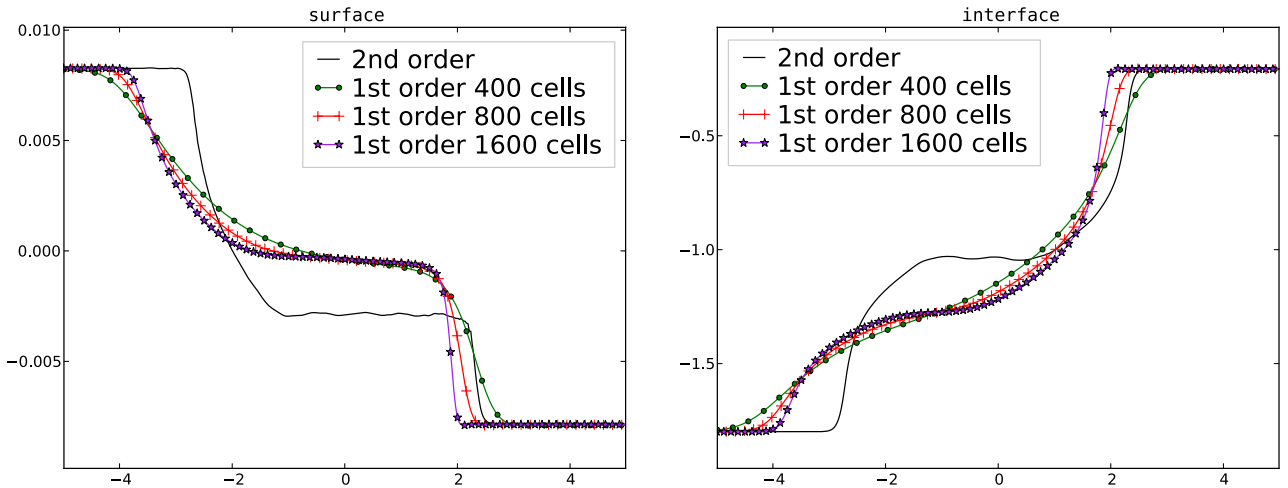


FIGURE 6. Same as in Figure 5, but for the CU scheme.

which correspond to an isolated internal shock wave traveling to the right.

In order to apply the CU scheme to the IVP (4.32), (5.1)–(5.3), we need (as in [36]) to rewrite the system (4.32) in the form (4.25) and properly select the constant Z_{ref} to ensure that $\varepsilon = h_1 + h_2 + Z_{\text{ref}}$ is relatively small. This is possible since according to (5.1)–(5.3) the jump in the water surface,

$$(h_1)_L + (h_2)_L - (h_1)_R - (h_2)_R = 0.01595,$$

is much smaller than the average water depth, which is

$$\frac{(h_1)_L + (h_2)_L + (h_1)_R + (h_2)_R}{2} = 1.971095.$$

The following three choices of Z_{ref} seem to be reasonable:

- (a) $Z_{\text{ref}} = -(h_1)_L - (h_2)_L$;
- (b) $Z_{\text{ref}} = -(h_1)_R - (h_2)_R$;
- (c) $Z_{\text{ref}} = -(h_1)_L - (h_2)_L + (h_1)_R + (h_2)_R / 2$.

In what follows below, we will refer to the CU schemes applied to the IVP (4.25), (5.1)–(5.3) with Z_{ref} given by one of the above options as CUa, CUb and CUc schemes, respectively. We would like to stress that as it has been shown in Section 4.2, the PCCU solution is independent of the reference water surface level, that is, of the choice of Z_{ref} .

We compute the solution of the IVP (4.32), (5.1)–(5.3) at the final time $t = 1$ by the PCCU, CUa, CUb and CUc schemes on the computational domain $[-1, 1]$ using the grid with 1000 uniform finite-volume cells. The obtained solutions $(h_1 + h_2)$ and h_2 are plotted in Figure 7, where it can clearly be seen that while the PCCU and CUc schemes produce almost the same numerical solutions, the results obtained using the other two versions of the CU scheme (CUa and CUb ones) are qualitatively different. This demonstrates an advantage of the PCCU scheme, which is independent of the choice of the reference water surface level.

In the second part of this numerical example, we follow the ideas presented in [15] and compare the analytical Hugoniot curve with the numerical ones. To this end, we fix the right state \mathbf{U}_R given by (5.2) and compute the set of the left states \mathbf{U}_L that can be connected to \mathbf{U}_R in the phase space through an internal shock.

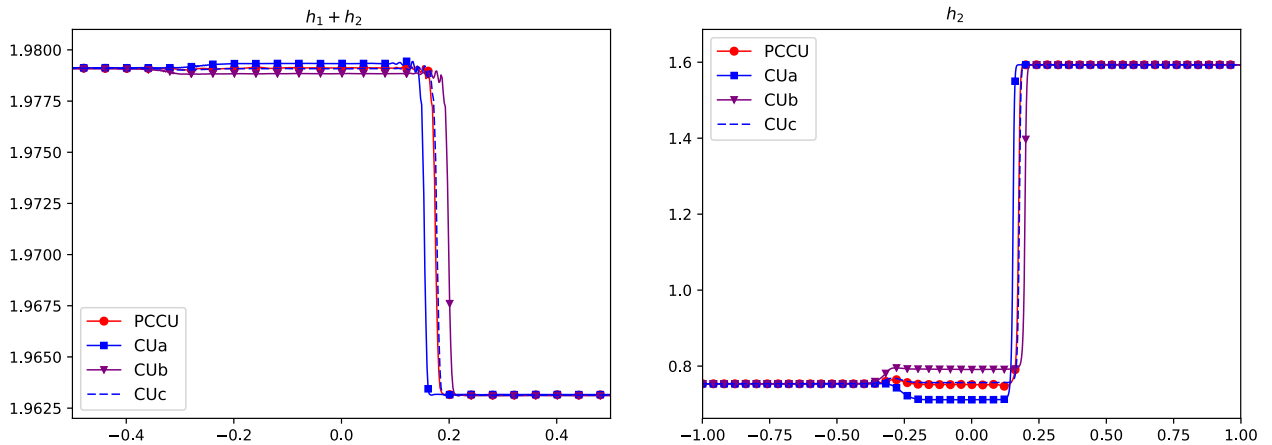


FIGURE 7. Example 5.3: $h_1 + h_2$ (left panel) and h_2 (right panel) computed using the PCCU, CUa, CUb and CUc schemes.

We first compute the analytical Hugoniot curve. According to the path-conservative theory [15, 20, 53], once a family of paths $\Psi(s; \mathbf{U}_L, \mathbf{U}_R)$ is selected, the shocks of the system should satisfy the generalized Rankine-Hugoniot condition

$$\mathbf{F}(\mathbf{U}_R) - \mathbf{F}(\mathbf{U}_L) - \int_0^1 B(\Psi(s; \mathbf{U}_L, \mathbf{U}_R)) \frac{d\Psi(s; \mathbf{U}_L, \mathbf{U}_R)}{ds} ds = \sigma(\mathbf{U}_R - \mathbf{U}_L), \quad (5.4)$$

where \mathbf{U}_L and \mathbf{U}_R are the left and right states that can be connected by a shock with speed σ . In particular, we will select the family of straight line paths and then (5.4) gives a one-parameter Hugoniot curve. The relation (5.4) has to be solved numerically for \mathbf{U}_L for different values of σ . Note that the right state (5.2) has been selected in such a way that the obtained \mathbf{U}_L correspond to an internal shock.

Next, we use the PCCU scheme to numerically solve the family of Riemann problems in which the right state is \mathbf{U}_R is given by (5.2) and \mathbf{U}_L runs along the Hugoniot curve. The speed of propagation and the limit states of the shock are then computed in these numerical solutions by using the first-order divided difference as a smoothness indicator. This computation has been performed using a uniform grid with 1000 cells in the interval $[-1, 1]$.

As it was stated in [15], one cannot expect the numerical solutions to converge to the weak shock solution even when the same family of paths is used both for the definition of the jump conditions and the construction of the numerical scheme. Moreover, one expects that the computed Hugoniot curve will diverge from the analytical one in the presence of strong shocks; see [15].

We then do the same for the CUa, CUb and CUc schemes. We recall that the right state (5.2) is such that the Hugoniot curve corresponds to an internal shock with a small jump at the water surface as can be seen in Figure 7 (left), where the computed solution ($h_1 + h_2$) for a particular left state \mathbf{U}_L on the Hugoniot curve is shown.

In Figure 8, we show the projection of the analytical and computed Hugoniot curves onto the h_1 - q_1 and h_2 - q_2 planes. We note that the PCCU scheme reproduces the analytical Hugoniot curve quite well although some differences may appear when the left state is far from the fixed right state. The situation with the CU schemes is quite different as only the Hugoniot curve computed by the CUc scheme agrees well with the analytical and PCCU Hugoniot curves. This means that the shocks obtained by the CU scheme will depend on the chosen reference level Z_{ref} , while the PCCU is independent of that choice and thus much more robust.

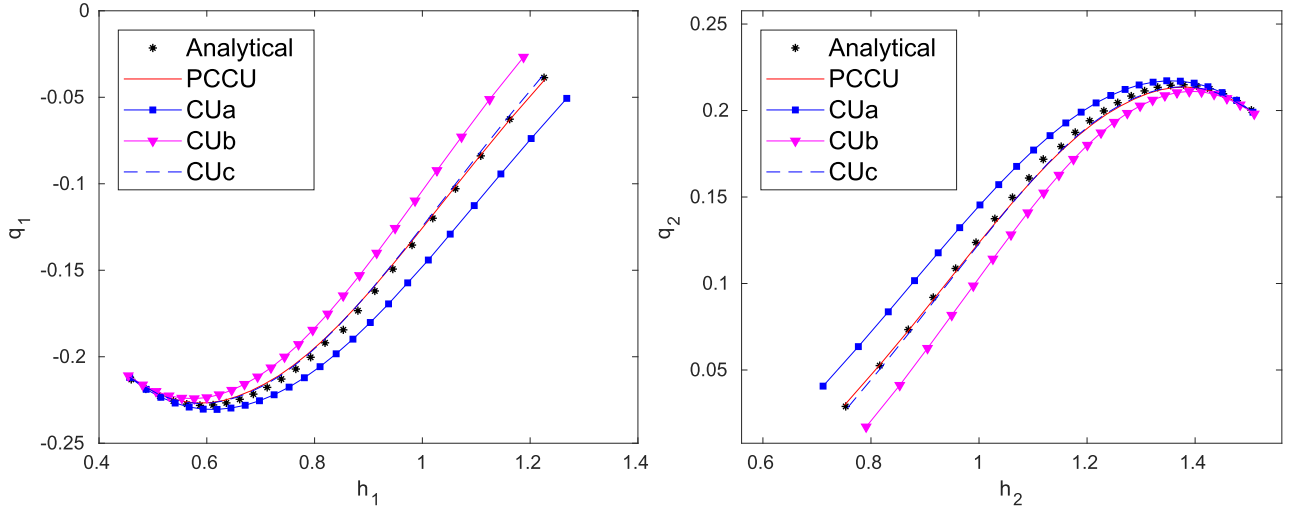


FIGURE 8. Example 5.3: projections onto the $h_1 - q_1$ (left panel) and $h_2 - q_2$ (right panel) planes of the analytical Hugoniot curve and four numerical ones, computed using the PCCU, CUa, CUb and CUc schemes.

Example 5.4 (Barotropic Tidal Flow). The last example is designed to mimic a tidal wave by imposing periodic in time boundary conditions at the left end of the computational domain.

We use the initial data (5.1) with

$$\mathbf{U}_R = ((h_1)_R, (q_1)_R, (h_2)_R, (q_2)_R)^T = (0.37002, -0.18684, 1.5931, 0.17416)^T$$

and

$$\mathbf{U}_L = ((h_1)_L, (q_1)_L, (h_2)_L, (q_2)_L)^T = (0.69914, -0.21977, 1.26932, 0.20656)^T,$$

which correspond to one of the internal shocks captured in Example 3 in order to construct the Hugoniot curve. We use a flat bottom topography and choose the reference water surface level

$$Z(x) \equiv Z_{\text{ref}} = -\frac{1}{2}((h_1)_L + (h_2)_L + (h_1)_R + (h_2)_R), \quad (5.5)$$

which was the best option for the CU scheme according to the numerical experiments conducted in Example 3.

We take the computational domain $[-10, 10]$ and impose open boundary conditions on the right and the following periodic in time boundary conditions on the left for the h_1 and h_2 components:

$$h_1(-10, t) = (h_1)_L + (h_1)_L \frac{0.03}{|Z_{\text{ref}}|} \sin\left(\frac{\pi t}{50}\right), \quad h_2(-10, t) = (h_2)_L + (h_1)_L \frac{0.03}{|Z_{\text{ref}}|} \sin\left(\frac{\pi t}{50}\right).$$

The values of q_1 and q_2 on the left edge of the computational domain are obtained by zero-order interpolation.

We numerically solve this initial-boundary value problem using the PCCU and CU and PCCU schemes on the grid with 1000 uniform finite-volume cells on the time interval $[0, 64]$. In Figure 9, we plot the solutions (water surface $\varepsilon = h_1 + h_2 + Z$ and interface $\omega = h_2 + Z$) computed at times $t = 10, 25, 60$ and 64 . As one can observe, both PCCU and CU solutions exhibit quite similar behavior at small times (even at time $t = 10$ the difference between the two solutions is not that significant). At larger times, however, the two schemes begin to produce very different results (for instance, at times $t = 25$ and 60 reported in Fig. 9). Moreover, for even larger times the CU solution begins to develop some spurious oscillations and will eventually become unstable. This is not the case for the PCCU solution which remains stable at all times.

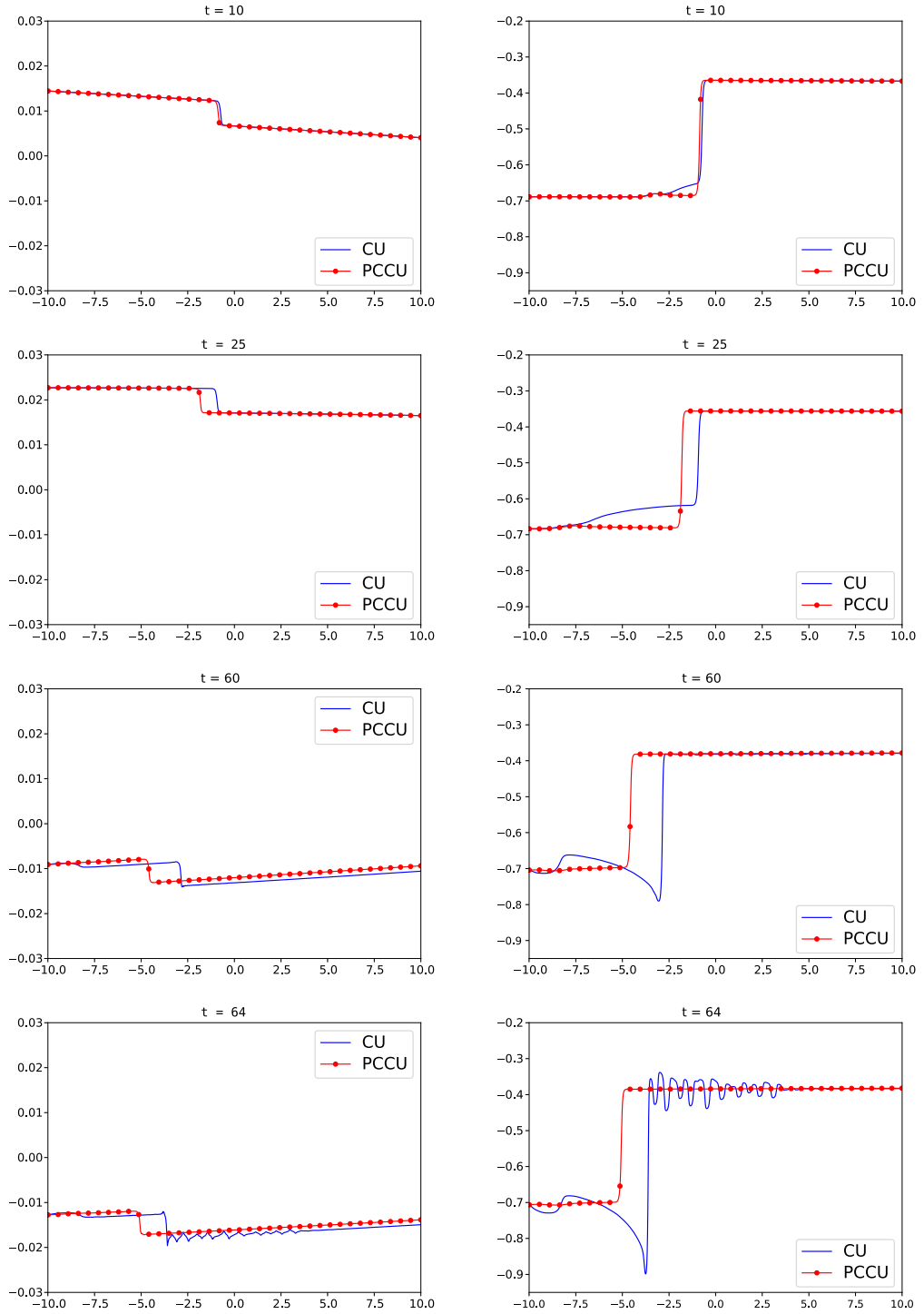


FIGURE 9. Example 5.4: water surface ε (left panel) and interface ω (right panel) computed using the PCCU and CU schemes at different times $t = 10, 25, 60$ and 64 .

We recall that in Example 5.3, the choice of the reference level (5.5) lead to the CU scheme (in fact, the CUC scheme) that produced the results similar to the PCCU ones. However, imposing the barotropic perturbation on the left boundary results in a totally different large time behavior of the solutions, computed by the two studied schemes. This is another strong evidence of the robustness of the proposed PCCU scheme.

6. CONCLUSION

In this paper, we develop PCCU schemes for nonconservative 1D hyperbolic systems of nonlinear PDEs. To this end, we rewrite the CU scheme in the form of path-conservative schemes showing that the main drawback of the original CU approach is the fact that the jump of the nonconservative product terms across cell interfaces is not taken into account. From the mathematical point of view, the path-conservative correction makes the numerical method to become formally consistent with a particular definition of weak solutions, while the original CU scheme is only consistent with smooth solutions. The formal consistency makes the PCCU scheme robust and helps to obtain better results than the original CU scheme.

We would also like to point out that when the terms that account for the contribution of the jumps of the nonconservative products at the cell interfaces are included, the first-order semi-discrete PCCU scheme coincides with the semi-discrete version of the path-conservative HLL solver.

The well-balanced property of the PCCU scheme is discussed and well-balanced PCCU solvers for both the single- and two-layer shallow-water systems are proposed.

Another important feature of the proposed PCCU schemes is related to the fact that application of the original CU scheme to the two-layer shallow-water system strongly depends on the formulation of the problem. A clear advantage of the proposed PCCU scheme is that when linear paths are considered, our scheme provides precisely the same discretization for both the original and modified formulations of the problem. In fact, this is a general property of path-conservative schemes, which are formally consistent with a particular definition of weak solution (given by the path) and therefore produce the same discretization independently of the formulation of the PDE provided the same conserved variables are used.

Finally, several numerical results clearly demonstrate a superb performance of the PCCU scheme, its robustness and ability to achieve very high resolution.

Acknowledgements. The work of Manuel Jesús Castro Díaz was supported in part by the Spanish Government and FEDER through the coordinated Research project MTM 2015-70490-C2-1-R. The work of A. Kurganov was supported in part by NSFC grant 11771201 and NSF grants DMS-1521009 and DMS-1818666. The work of Tomás Morales de Luna was supported in part by the Spanish Government and FEDER through the coordinated Research project MTM 2015-70490-C2-2-R.

REFERENCES

- [1] R. Abgrall and S. Karni, Two-layer shallow water system: a relaxation approach. *SIAM J. Sci. Comput.* **31** (2009) 1603–1627.
- [2] R. Abgrall and S. Karni, A comment on the computation of non-conservative products. *J. Comput. Phys.* **229** (2010) 2759–2763.
- [3] P. Arminjon, M.-C. Viallon and A. Madrane, A finite volume extension of the Lax–Friedrichs and Nessyahu–Tadmor schemes for conservation laws on unstructured grids. *Int. J. Comput. Fluid Dyn.* **9** (1997) 1–22.
- [4] E. Audusse, F. Bouchut, M.-O. Bristeau, R. Klein and B. Perthame, A fast and stable well-balanced scheme with hydrostatic reconstruction for shallow water flows. *SIAM J. Sci. Comput.* **25** (2004) 2050–2065.
- [5] C. Berthon and F. Marche, A positive preserving high order VFRoe scheme for shallow water equations: a class of relaxation schemes. *SIAM J. Sci. Comput.* **30** (2008) 2587–2612.
- [6] F. Bianco, G. Puppo and G. Russo, High order central schemes for hyperbolic systems of conservation laws. *SIAM J. Sci. Comput.* **21** (1999) 294–322.
- [7] A. Bollermann, G. Chen, A. Kurganov and S. Noelle, A well-balanced reconstruction of wet/dry fronts for the shallow water equations. *J. Sci. Comput.* **56** (2013) 267–290.
- [8] A. Bollermann, S. Noelle and M. Lukáčová-Medviďová, Finite volume evolution Galerkin methods for the shallow water equations with dry beds. *Commun. Comput. Phys.* **10** (2011) 371–404.
- [9] F. Bouchut, Nonlinear stability of finite volume methods for hyperbolic conservation laws and well-balanced schemes for sources. *Frontiers in Mathematics*. Birkhäuser Verlag, Basel (2004).

- [10] F. Bouchut and T. Morales de Luna, An entropy satisfying scheme for two-layer shallow water equations with uncoupled treatment. *ESAIM: M2AN* **42** (2008) 683–698.
- [11] F. Bouchut and V. Zeitlin, A robust well-balanced scheme for multi-layer shallow water equations. *Discrete Contin. Dyn. Syst. Ser. B* **13** (2010) 739–758.
- [12] S. Bryson, Y. Epshteyn, A. Kurganov and G. Petrova, Well-balanced positivity preserving central-upwind scheme on triangular grids for the Saint-Venant system. *ESAIM: M2AN* **45** (2011) 423–446.
- [13] M. Castro, J. Macías and C. Parés, A Q -scheme for a class of systems of coupled conservation laws with source term. Application to a two-layer 1-D shallow water system. *ESAIM: M2AN* **35** (2001) 107–127.
- [14] M. Castro, A. Pardo, C. Parés and E. Toro, On some fast well-balanced first order solvers for nonconservative systems. *Math. Comput.* **79** (2010) 1427–1472.
- [15] M.J. Castro, P.G. LeFloch, M.L. Muñoz-Ruiz and C. Parés, Why many theories of shock waves are necessary: convergence error in formally path-consistent schemes. *J. Comput. Phys.* **227** (2008) 8107–8129.
- [16] M.J. Castro, T. Morales de Luna and C. Parés, Well-balanced schemes and path-conservative numerical methods. Handbook of Numerical Methods for Hyperbolic Problems. In Vol. 18 of Handbook of Numerical Analysis. Elsevier/North-Holland, Amsterdam (2017) 131–175.
- [17] M. Castro Díaz and E. Fernández-Nieto, A class of computationally fast first order finite volume solvers: PVM methods. *SIAM J. Sci. Comput.* **34** (2012) A2173–A2196.
- [18] J.-J. Cauret, J.-F. Colombeau and A.Y. LeRoux, Discontinuous generalized solutions of nonlinear nonconservative hyperbolic equations. *J. Math. Anal. Appl.* **139** (1989) 552–573.
- [19] A. Chertock, A. Kurganov, Z. Qu and T. Wu, Three-layer approximation of two-layer shallow water equations. *Math. Model. Anal.* **18** (2013) 675–693.
- [20] G. Dal Maso, P.G. Lefloch and F. Murat, Definition and weak stability of nonconservative products. *J. Math. Pures Appl.* **74** (1995) 483–548.
- [21] A. de Saint-Venant, Théorie du mouvement non-permanent des eaux, avec application aux crues des rivières et à l'introduction des marées dans leur lit. *C.R. Acad. Sci. Paris* **73** (1871) 147–154.
- [22] M. Dumbser, A. Hidalgo and O. Zanotti, High order space-time adaptive ADER-WENO finite volume schemes for non-conservative hyperbolic systems. *Comput. Methods Appl. Mech. Eng.* **268** (2014) 359–387.
- [23] U.S. Fjordholm, S. Mishra and E. Tadmor, Well-balanced and energy stable schemes for the shallow water equations with discontinuous topography. *J. Comput. Phys.* **230** (2011) 5587–5609.
- [24] K.O. Friedrichs, Symmetric hyperbolic linear differential equations. *Commun. Pure Appl. Math.* **7** (1954) 345–392.
- [25] S. Gottlieb, D. Ketcheson and C.-W. Shu, Strong Stability Preserving Runge–Kutta and Multistep Time Discretizations. World Scientific Publishing Co. Pte. Ltd. Hackensack, NJ (2011).
- [26] S. Gottlieb, C.-W. Shu and E. Tadmor, Strong stability-preserving high-order time discretization methods. *SIAM Rev.* **43** (2001) 89–112.
- [27] A. Harten, P. Lax and B. van Leer, On upstream differencing and Godunov-type schemes for hyperbolic conservation laws. *SIAM Rev.* **25** (1983) 35–61.
- [28] G.-S. Jiang and E. Tadmor, Nonoscillatory central schemes for multidimensional hyperbolic conservation laws. *SIAM J. Sci. Comput.* **19** (1998) 1892–1917.
- [29] A. Kurganov, Well-balanced central-upwind scheme for compressible two-phase flows. In: *Proceedings of the European Conference on Computational Fluid Dynamics ECCOMAS CFD* (2006).
- [30] A. Kurganov, Central schemes: a powerful black-box solver for nonlinear hyperbolic PDEs. Handbook of Numerical Methods for Hyperbolic Problems. In Vol. 17 of Handbook of Numerical Analysis. Elsevier/North-Holland, Amsterdam (2016) 525–548.
- [31] A. Kurganov and D. Levy, Central-upwind schemes for the Saint-Venant system. *ESAIM: M2AN* **36** (2002) 397–425.
- [32] A. Kurganov and C.-T. Lin, On the reduction of numerical dissipation in central-upwind schemes. *Commun. Comput. Phys.* **2** (2007) 141–163.
- [33] A. Kurganov and J. Miller, Central-upwind scheme for Savage–Hutter type model of submarine landslides and generated tsunami waves. *Comput. Methods Appl. Math.* **14** (2014) 177–201.
- [34] A. Kurganov, S. Noelle and G. Petrova, Semi-discrete central-upwind scheme for hyperbolic conservation laws and Hamilton–Jacobi equations. *SIAM J. Sci. Comput.* **23** (2001) 707–740.
- [35] A. Kurganov and G. Petrova, A second-order well-balanced positivity preserving central-upwind scheme for the Saint-Venant system. *Commun. Math. Sci.* **5** (2007) 133–160.
- [36] A. Kurganov and G. Petrova, Central-upwind schemes for two-layer shallow equations. *SIAM J. Sci. Comput.* **31** (2009) 1742–1773.
- [37] A. Kurganov, M. Prugger and T. Wu, Second-order fully discrete central-upwind scheme for two-dimensional hyperbolic systems of conservation laws. *SIAM J. Sci. Comput.* **39** (2017) A947–A965.
- [38] A. Kurganov and E. Tadmor, New high resolution central schemes for nonlinear conservation laws and convection-diffusion equations. *J. Comput. Phys.* **160** (2000) 241–282.
- [39] J.L. Lagrange, Traité de la résolution des équations numériques, Paris 1798. Reprinted in Œuvres complètes, tome 8. Gallica (1879).
- [40] P.D. Lax, Weak solutions of nonlinear hyperbolic equations and their numerical computation. *Commun. Pure Appl. Math.* **7** (1954) 159–193.

- [41] P.G. LeFloch, Hyperbolic systems of conservation laws. The theory of classical and nonclassical shock waves. *Lectures in Mathematics* ETH Zürich. Birkhäuser Verlag, Basel (2002).
- [42] P.G. LeFloch, Graph solutions of nonlinear hyperbolic systems. *J. Hyperbolic Differ. Equ.* **1** (2004) 643–689.
- [43] R.J. LeVeque, Balancing source terms and flux gradients in high-resolution Godunov methods: the quasi-steady wave-propagation algorithm. *J. Comput. Phys.* **146** (1998) 346–365.
- [44] D. Levy, G. Puppo and G. Russo, A fourth-order central WENO scheme for multidimensional hyperbolic systems of conservation laws. *SIAM J. Sci. Comput.* **24** (2002) 480–506.
- [45] K.-A. Lie and S. Noelle, An improved quadrature rule for the flux-computation in staggered central difference schemes in multidimensions. *J. Sci. Comput.* **63** (2003) 1539–1560.
- [46] K.-A. Lie and S. Noelle, On the artificial compression method for second-order nonoscillatory central difference schemes for systems of conservation laws. *SIAM J. Sci. Comput.* **24** (2003) 1157–1174.
- [47] X.-D. Liu and E. Tadmor, Third order nonoscillatory central scheme for hyperbolic conservation laws. *Numer. Math.* **79** (1998) 397–425.
- [48] J. Macías, C. Pares and M.J. Castro, Improvement and generalization of a finite element shallow-water solver to multi-layer systems. *Int. J. Numer. Methods Fluids* **31** (1999) 1037–1059.
- [49] J.-M. Masella, I. Faille and T. Gallouët, On an approximate Godunov scheme. *Int. J. Comput. Fluid Dyn.* **12** (1999) 133–149.
- [50] M. Mignotte and D. Stefanescu, On an Estimation of Polynomial Roots by Lagrange. Tech. Report 025/2002. IRMA Strasbourg (2002) 1–17. Available at: <http://hal.archives-ouvertes.fr/hal-00129675/en/>.
- [51] M.L. Muñoz-Ruiz and C. Parés, On the convergence and well-balanced property of path-conservative numerical schemes for systems of balance laws. *J. Sci. Comput.* **48** (2011) 274–295.
- [52] H. Nessyahu and E. Tadmor, Nonoscillatory central differencing for hyperbolic conservation laws. *J. Comput. Phys.* **87** (1990) 408–463.
- [53] C. Parés, Numerical methods for nonconservative hyperbolic systems: a theoretical framework. *SIAM J. Numer. Anal.* **44** (2006) 300–321.
- [54] C. Parés, Path-conservative numerical methods for nonconservative hyperbolic systems. In: Numerical Methods for Balance Laws. *Quad. Mat. Dept. Math. Seconda Univ. Napoli, Caserta* **24** (2009) 67–121.
- [55] C. Parés and M. Castro, On the well-balance property of Roe's method for nonconservative hyperbolic systems. Applications to shallow-water systems. *ESAIM: M2AN* **38** (2004) 821–852.
- [56] P. Roe, Approximate Riemann solvers, parameter vectors, and difference schemes. *J. Comput. Phys.* **43** (1981) 357–372.
- [57] J. Schijf and J. Schonfeld, Theoretical considerations on the motion of salt and fresh water. In: *Proceedings, Minnesota International Hydraulics Convention* (1953) 321–333.
- [58] C.-W. Shu, High order weighted essentially nonoscillatory schemes for convection dominated problems. *SIAM Rev.* **51** (2009) 82–126.
- [59] B. van Leer, Towards the ultimate conservative difference scheme. V. A second-order sequel to Godunov's method. *J. Comput. Phys.* **32** (1979) 101–136.
- [60] A.I. Vol'pert, Spaces BV and quasilinear equations. *Mat. Sb. (N.S.)* **73** (1967) 255–302.